Published in final edited form as:
Nat Cell Biol. 2021 June 01; 23(6): 608–619. doi:10.1038/s41556-021-00692-z.

Elongation factor ELOF1 drives transcription-coupled repair and prevents genome instability

Marit E Geijer[1], **Di Zhou**[#1], **Kathiresan Selvam**[#2], **Barbara Steurer**[#1], **Chirantani Mukherjee**[#1], **Bastiaan Evers**[#3], **Simona Cugusi**[#4], **Marvin van Toorn**[1], **Melanie van der Woude**[1], **Roel C. Janssens**[1], **Yannick P Kok**[5], **Wenzhi Gong**[6], **Anja Raams**[1], **Calvin SY Lo**[1], **Joyce HG Lebbink**[1,7], **Bart Geverts**[8], **Dalton A Plummer**[2], **Karel Bezstarosti**[9], **Arjan F Theil**[1], **Richard Mitter**[10], **Adriaan B Houtsmuller**[8], **Wim Vermeulen**[1], **Jeroen AA Demmers**[9], **Shisheng Li**[6], **Marcel ATM van Vugt**[5], **Hannes Lans**[1], **René Bernards**[3], **Jesper Q Svejstrup**[4], **Arnab Ray Chaudhuri**[1], **John J Wyrick**[2], **Jurgen A Marteijn**[1,*]

[1]Department of Molecular Genetics, Oncode Institute, Erasmus MC Cancer Institute, Erasmus University Medical Center, Rotterdam, the Netherlands [2]School of Molecular Biosciences, Washington State University, Pullman, Washington 99164, USA [3]Oncode Institute, Division of Molecular Carcinogenesis, The Netherlands Cancer Institute, Amsterdam, The Netherlands [4]Mechanisms of Transcription Laboratory, The Francis Crick Institute, 1 Midland Road, London NW1 1AT, UK [5]Department of Medical Oncology, University Medical Center Groningen, University of Groningen, Groningen, The Netherlands [6]Department of Comparative Biomedical Sciences, School of Veterinary Medicine, Louisiana State University, Baton Rouge, LA, 70803, USA [7]Department of Radiation Oncology, Erasmus University Medical Center, Rotterdam, The Netherlands [8]Erasmus Optical Imaging Center, Erasmus University Medical Center Rotterdam, Rotterdam, The Netherlands [9]Proteomics Center, Erasmus University Medical Center, Rotterdam, the Netherlands [10]Bioinformatics and Biostatistics, The Francis Crick Institute, 1 Midland Road, London NW1 1AT, UK

[#] These authors contributed equally to this work.

Abstract

[*]Correspondence should be addressed to J.A.M. (J.Marteijn@eramusmc.nl).

Author contributions: M.E.G performed the majority of the experiments and generated ELOF1 and CSB KO cell lines and ELOF1- and RPB1-KI cell lines. D.Z. generated CSB- and UVSSA-KI cells and performed live-cell imaging experiments and the TCR-UDS. K.S., D.A.P., W.G., S.L., and J.J.W. performed and supervised all experiments in *S. cerevisiae*. B.S. and M.E.G. performed the CRISPR/cas9 screen, and B.E. and R.B. analyzed and supervised the screen. C.M., S.L. and A.R.C. performed and supervised the metaphase spread, DNA fiber analysis and 53BP1 cell cycle analysis. S.C., R.M., and J.Q.S. performed and supervised the DRB/TT_{chem}-seq. M.v.T. performed the alamar blue cell viability assay. M.v.d.W. and H.L. performed and supervised the experiments in *C. elegans*. R.J. provided experimental support. Y.K. performed EdU and FANCD2 foci analysis, supervised by M.v.V. J.L. generated images of Pol II structure. B.G. performed Monte-Carlo based-modeling and was supervised by A.H. K.B. and J.A.A.D. performed and supervised mass spectrometry analysis. A.R. performed UDS experiments and A.F.T. performed FACS sorting, both supervised by W.V. J.A.M. conceived and supervised the project and together with M.E.G. wrote the manuscript with input from all authors.

Competing interests:
Authors declare no competing interests.

Europe PMC Funders Author Manuscripts

Correct transcription is crucial for life. However, DNA damage severely impedes elongating RNA Polymerase II (Pol II), causing transcription inhibition and transcription-replication conflicts. Cells are equipped with intricate mechanisms to counteract the severe consequence of these transcription-blocking lesions (TBLs). However, the exact mechanism and factors involved remain largely unknown. Here, using a genome-wide CRISPR/cas9 screen, we identified elongation factor ELOF1 as an important factor in the transcription stress response upon DNA damage. We show that ELOF1 has an evolutionary conserved role in Transcription-Coupled Nucleotide Excision Repair (TC-NER), where it promotes recruitment of the TC-NER factors UVSSA and TFIIH to efficiently repair TBLs and resume transcription. Additionally, ELOF1 modulates transcription to protect cells from transcription-mediated replication stress, thereby preserving genome stability. Thus, ELOF1 protects the transcription machinery from DNA damage via two distinct mechanisms.

Introduction

Faithful transcription is essential for proper cell function. However, transcription is continuously threatened by DNA-damaging agents, which induce transcription-blocking lesions (TBLs) that strongly impede or completely block progression of RNA polymerase II (Pol II). Impeded transcription elongation by DNA damage can affect transcription fidelity or result in complete absence of newly synthesized mRNA transcripts. This can result in severe cellular dysfunction, senescence and cell death, consequently contributing to aging[1]. Furthermore, prolonged stalling of Pol II at TBLs can form an obstacle for the replication machinery, thereby giving rise to transcription-replication conflicts. These conflicts can lead to genome instability and onset of cancer[2, 3]. Cells are equipped with an intricately regulated cellular response to overcome these severe consequences of TBLs. This transcription stress response includes repair of TBLs and mechanisms to overcome transcription-replication conflicts[1, 2].

The main mechanism to remove TBLs is transcription-coupled nucleotide excision repair (TC-NER). TC-NER removes a wide spectrum of environmentally or endogenously-induced TBLs, including UV light-induced lesions an oxidative damage[1]. The biological relevance of TC-NER is best illustrated by Cockayne syndrome (CS), which is characterized by photosensitivity, progressive neurodegeneration and premature aging[4], and is caused by inactivating mutations in TC-NER genes. The TC-NER initiating factor CSB (ERCC6) is recruited upon Pol II stalling. CSB uses its forward translocating ability to discriminate between lesion-stalled and other forms of paused Pol II[5]. When lesion-stalled Pol II is recognized, the full TC-NER complex is assembled by the recruitment of CSA (ERCC8), which is part of a Cullin 4-RING E3 ubiquitin ligase complex ($CRL4^{CSA}$)[6], and UVSSA[7]. Recently it was shown that the ubiquitylation of lesion-stalled Pol II plays an important role in TC-NER complex assembly and in the transcription stress response[8, 9]. UVSSA subsequently promotes the recruitment of TFIIH[7, 10], which forms the core incision complex with XPA and RPA. This complex recruits the endonucleases ERCC1/XPF and XPG to excise the TBL[11]. Repair is finalized by refilling and ligating the gap, after which transcription can restart[1].

Europe PMC Funders Author Manuscripts

Although several key factors have been identified in the cellular response to DNA damage-induced transcription stress, the exact molecular mechanism how cells repair TBLs and avoid collisions of lesion-stalled Pol II with the replication machinery remain largely unknown.

Results

ELOF1 protects against UV-induced DNA damage

To identify factors involved in the DNA damage-induced transcription stress response, we performed a genome-wide CRISPR/Cas9 loss-of-function screen following UV-induced DNA damage. Briefly, fibroblasts were transduced with a lentiviral sgRNA library[12] and UV-irradiated for 10 consecutive days (Fig.1a, Extended data Fig.1a). sgRNA abundance was determined by next-generation sequencing and was compared to untreated cells using MAGeCK analysis[13] (Fig.1b, Extended data Table 1). Gene ontology analysis among the top UV-sensitive hits (FDR<0.1), identified many genes involved in the UV-induced DNA damage response (Extended data Fig.1b), such as translesion synthesis (TLS) factors[14], and many NER genes[11]. Especially the identification of the key TC-NER factors *CSA, CSB* and *UVSSA* underscored the potential of this screen to identify factors involved in the DNA damage-induced transcription stress response.

One of the top UV-sensitive hits was Elongation Factor 1 Homolog (*ELOF1*), an evolutionary-conserved small zinc-finger protein (~10 kDa)[15]. Its orthologue, *ELF1*, was identified in budding yeast where its disruption was synthetically lethal with mutations in genes encoding elongation factors such as *SPT6* and *TFIIS* [16]. Follow-up studies in yeast revealed that Elf1 interacts with the elongation complex[16-19] and i*n vitro* studies showed that Elf1 binds downstream of Pol II at the DNA entry tunnel and promotes elongation through nucleosomes[20]. However, its exact function and its role in the DNA damage response thus far remained unknown.

To validate the UV-sensitivity upon ELOF1 depletion, we performed clonogenic survival experiments using two independent ELOF1 knockout (KO) HCT116 cell lines (Extended data Fig.1c-g). ELOF1 deficiency resulted in a severe UV hypersensitivity, to the same level as in TC-NER-deficient CSB KO cells (Fig.1c). Similar results were obtained upon siRNA-mediated ELOF1 depletion (Fig.1d, Extended data Fig.1h,i). ELOF1 re-expression in ELOF1 KO cells fully rescued UV sensitivity, indicating that the observed effects are specific for ELOF1. Although the N-terminal tail of ELOF1 promotes Pol II progression on the nucleosome[20], absence of this tail could still rescue the UV sensitivity (Fig.1f, Extended data Fig.1j). However, the conserved zinc-finger domain of ELOF1 was crucial for UV survival. Furthermore, photolyase-mediated reversal[21] of UV-induced cyclobutane pyrimidine dimers (CPD) almost completely rescued the UV sensitivity of ELOF1 KO cells, showing that this sensitivity is due to DNA damage and not RNA or protein damage (Extended data Fig.1k).

ELOF1 is a transcription elongation factor

We first tested whether ELOF1 is part of the elongating Pol II complex, as previously observed in yeast[16–20]. We generated homozygous *ELOF1-mScarletI-HA* knock-in (KI) cells to detect endogenously expressed ELOF1 (Extended data Fig.2a). ELOF1 was localized strictly to the nucleus, excluded from the nucleoli, and showed high level of co-localization with Pol II (Fig.2a and Extended data Fig.2b,c). Live-cell imaging studies on GFP-RPB1 mobility showed that fluorescence recovery after photobleaching (FRAP) experiments are a sensitive way to study Pol II-mediated transcription[22]. Therefore, we compared the mobility of ELOF1 to that of Pol II, and observed that it was almost identical in non-treated conditions (Fig.2b). The large ELOF1 immobilization, suggests that the majority of ELOF1 molecules are chromatin-bound, most likely engaged in transcription elongation, similar as observed for Pol II[22]. The engagement of ELOF1 in transcription elongation was confirmed by its swift chromatin release, as shown by its strong mobilization upon transcription inhibition (Fig.2b). This almost complete mobilization suggests that ELOF1 is exclusively involved in transcription-related processes.

To further investigate whether ELOF1 is part of the elongating Pol II complex, we immunoprecipitated (IP) ELOF1 and showed its interaction with RPB1 and RPB3, subunits of Pol II (Fig.2c). The interaction of ELOF1 with P-Ser2-modified RPB1, which primarily marks elongating Pol II, indicates that ELOF1 is present in the elongation complex, which was confirmed by the reciprocal IP (Extended data Fig.2d). Moreover, SILAC-based interaction proteomics of endogenously expressed GFP-RPB1[22] identified ELOF1 as a Pol II-interactor with similar SILAC ratios as other elongation factors (Extended data Fig.2e, Extended data Table 2). To obtain a complete overview of ELOF1-interacting proteins, we performed SILAC-based interaction proteomics for ELOF1, revealing high SILAC ratios for many Pol II subunits and elongation factors including TFIIS, SPT5, SPT6 and the PAF complex (Fig.2d, Extended data Table 2). Gene ontology analysis of ELOF1-interactors revealed its involvement in transcription-related processes (Extended data Fig.2f). Of note, the ELOF1-Pol II interaction did not change upon UV-induced DNA damage, in contrast to the Pol II-CSB interaction[23] (Fig.2c and Extended data Fig.2d). These data indicate that ELOF1 is an integral component of the transcription elongation complex, independent of DNA damage.

Next, we tested whether ELOF1 acts as a transcription elongation factor by determining its effect on Pol II elongation rates using DRB/TT_{chem}-seq[24]. Nascent RNA was labeled with 4SU to determine the Pol II position in gene bodies at different time points after its release from the promoter by DRB washout (Fig.2e). Single gene profiles (Extended data Fig.3a) and metagene analysis of >200kb genes (Fig.2e,f) showed that ELOF1 KO resulted in a clear decreased average elongation rate from 2.6 kb/min to 2.0 kb/min, while ~6-fold overexpression of ELOF1 (Extended data Fig.1f) resulted in an increased average elongation rate to 3.1 kb/min. In contrast, loss of CSB had no obvious effect on Pol II elongation rate. Comparable results were obtained for shorter genes (Extended data Fig.3a,b). In line with this reduced elongation rate, the overall nascent RNA synthesis was also reduced upon ELOF1 depletion (Extended data Fig.3c-e).

To obtain mechanistic insights in the reduced elongation speed in ELOF1 KO cells, we studied the differences in the P-Ser2-modified Pol II interactome with and without ELOF1 using SILAC-based proteomics. Absence of ELOF1 did not affect the presence of the core Pol II subunits or the majority of elongation factors (Fig.2g, Extended data Table 2). Interestingly, the biggest change in complex composition was found for CSA and CSB, each having a 4-fold increased Pol II interaction without ELOF1. Increased CSB binding might indicate that Pol II forward translocation is more frequently perturbed without ELOF1, since CSB recognizes stalled Pol II at DNA lesions and natural pause sites[5]. Such perturbation can stimulate Pol II backtracking and recruitment of TFIIS to stimulate transcript cleavage and transcription resumption[25]. In line with this, we observed an increased TFIIS binding to elongating Pol II in ELOF1 KO cells (Fig.2g). Furthermore, depletion of TFIIS gave rise to synthetic lethality with ELOF1 KO (Extended data Fig.3f), as was also observed in yeast[16].

ELOF1 is essential for TC-NER

After having established that ELOF1 is a *bona fide* elongation factor, we studied its role in the DNA damage response. Since ELOF1 KO cells are sensitive for UV-induced DNA damage, which is a potent inhibitor of transcription, we tested whether ELOF1 is needed for recovery of transcription after UV, by quantifying nascent transcription levels by EU incorporation[26]. Transcription was severely inhibited 2 hours after UV but fully recovered in Wt cells after 18 hours (Fig.3a, Extended data Fig.4a). The transcription recovery was completely abolished in ELOF1 KO cells, similar as in TC-NER-deficient CSA KO cells, but could be rescued by re-expression of ELOF1. Similar results were obtained using siRNA-mediated ELOF1 knockdown (Extended data Fig.4b,c). To distinguish whether ELOF1 has a specific function in the restart of transcription, or is also involved in TBL removal, we measured TC-NER activity by quantifying the gap-filling synthesis using EdU incorporation in non-replicating GG-NER-deficient cells[27]. Like CSB depletion, loss of ELOF1 severely inhibited TC-NER activity (Fig.3b, Extended data Fig.4d,e). The function of ELOF1 was restricted to the TC-NER sub-pathway, since the gap-filling synthesis in GG-NER-proficient cells was not affected (Fig.3c, Extended data Fig.4f,g). Together, this shows that ELOF1 has a crucial function in TC-NER to subsequently promote transcription recovery.

Then, we tested the sensitivity of ELOF1 KO cells to other types of DNA damage. ELOF1 KO cells, like CSB KO cells, displayed severe sensitivity to a wide spectrum of genotoxins that cause TBLs, including Illudin S[28], Cisplatin[29], Camptothecin[30] and oxidative lesions[31] (Fig.3d,e, Extended data Fig.4h-j). However, ELOF1 KO cells were not sensitive to replication stress induced by hydroxyurea or aphidicolin (Extended data Fig.4k,l). Importantly, depletion of elongation factors does not generally induce sensitivity to TBLs. For example, knockdown of the elongation factors SPT4/5 did not induce UV sensitivity, although this reduced RNA synthesis to a similar extent as ELOF1 depletion (Extended data Fig.3c-e, 4m).

ELOF1 is an evolutionary conserved TC-NER factor

As *ELOF1* is highly conserved from archaea to mammals[15], we tested whether the *ELOF1* orthologues in *Saccharomyces cerevisiae* and *Caenorhabditis elegans* are also involved in

TC-NER. Similar to mutations in *RAD26,* the budding yeast ortholog of *CSB*, inactivation of *ELF1* (*elf1Δ*) had no effect on UV sensitivity (Extended data Fig.5a), which is explained by the efficient GG-NER machinery[32]. Therefore, we studied the effect of *elf1Δ* in TC-NER, in GG-NER-deficient *RAD16* mutants (*rad16Δ*). This showed strong UV-sensitivity for *elf1Δ*, like *rad26Δ* mutants (Fig.4a).

To determine if the increased UV sensitivity in the *elf1Δ* mutant is caused by a TC-NER-defect, we analyzed CPD repair profiles in the transcribed strand (TS) and non-transcribed strand (NTS) of yeast genes 2 hours after UV using high-resolution CPD-sequencing[33] (Extended data Fig.5b). Meta-analysis of ~5000 genes (Fig.4b) and by individual genes (Extended data Fig.5c) showed that, in the *elf1Δ* mutant, GG-NER-mediated repair in the NTS was hardly affected while TC-NER-mediated repair in the TS was severely compromised. Global repair in *elf1Δ* was hardly affected (Extended data Fig.5d), which is in agreement with TC-NER-specific repair that only happens in the TS of active genes. Although Elf1 was described to stimulate Pol II progression on the nucleosome[20], no nucleosome-dependent difference in TC-NER efficiency was detected in the TS in *elf1Δ* mutants (Extended data Fig.5e).

Strikingly, the *elf1Δ rad26Δ* double mutant showed an even higher UV sensitivity than the single mutants in a *rad16Δ* background, indicating that Elf1 has functions independent of Rad26 (Fig.4a). Close-ups of the CPD-seq data showed that repair immediately downstream of the transcription start site (TSS) was compromised in the *elf1Δ* mutant (Fig.4c). This genomic region can be repaired in a Rad26-independent manner[34] by an Rpb9-mediated transcription-coupled repair mechanism[35] and suggests a role for Elf1 in this pathway. Indeed, *elf1*Δ enhances the UV sensitivity in a *rad16Δrpb9Δ* mutant, but not in a *rad16Δrpb9Δrad26* mutant (Fig.4d and Extended data Fig.5f), indicating that Elf1 is involved in both Rad26-dependent and Rpb9-dependent repair. This was confirmed by reduced TC-NER in both *rad16Δrad26Δ* and *rad16Δrpb9Δ* mutants after deletion of *ELF1* (Extended data Fig.5g,h).

To study the role of ELOF1 in a multi-cellular model organism, we made use of the conservation of *ELOF1* in *C. elegans*. We assayed UV-survival of mutant germ and early embryonic cells, which predominantly depends on GG-NER, and of post-mitotic first-stage larvae, which mainly depends on TC-NER[36]. Inactivation of *elof-1* (Extended data Fig.5i) did not increase UV sensitivity of germ and embryonic cells, in contrast to inactivation of the GG-NER factor *xpc-1,* (Fig.4e). However, *elof-1* animals showed a strong UV sensitivity in the first larval stage, similar to TC-NER-deficient *csb-1* animals (Fig.4f), showing that ELOF1 is an evolutionary conserved TC-NER factor.

Pol II progression is impaired in ELOF1-deficient cells upon UV

As the TC-NER factor ELOF1 is an integral part of the elongation complex, its depletion will likely affect Pol II progression upon encountering TBLs. To test this, we used GFP-RPB1 KI cells to study Pol II mobility by FRAP, which provides quantitative information on Pol II elongation rates and fraction sizes of elongating and promoter-bound Pol II[22]. UV-induced DNA damage increased the Pol II immobilization, especially of the long-bound elongating fraction, as evident from the reduced slope of the FRAP curve at time points

>100 sec (Fig.5a)[22]. Monte-Carlo-based modeling revealed an increased fraction size and residence time of elongating Pol II, indicating that UV-exposure resulted in more elongating Pol II that transcribes slower (Fig.5b), likely caused by Pol II-stalling at TBLs[37]. Upon knockdown of ELOF1, elongating Pol II was further immobilized following UV, to a similar extent as after depletion of CSB. The average residence time of elongating Pol II in ELOF1-depleted cells increased ~30%, suggesting that Pol II-stalling at lesions is prolonged (Fig.5a,b, Extended data Fig.6a). Similar results were obtained by Pol II ChIP-seq experiments (van der Weegen *et al.* submitted back-to-back). ELOF1 knockdown also resulted in an increased residence time of elongating Pol II in unperturbed conditions, indicative of a reduced elongation rate (Extended data Fig.6b,c), in line with our DRB/TT_{chem}-seq data (Fig.2e,f).

ELOF1 stimulates Pol II ubiquitylation and recruitment of UVSSA and TFIIH during TC-NER

To study TC-NER complex assembly, we performed SILAC-based interaction proteomics on P-Ser2-modified Pol II after UV in the presence or absence of ELOF1. Pol II interaction with most elongation factors remained unaffected in absence of ELOF1 (Fig.5c, Extended data Fig.6d and Extended data Table 2). Interestingly, while CSA and CSB could still bind Pol II in the absence of ELOF1, binding of UVSSA and the TFIIH subunits was severely compromised. These results were confirmed by IP experiments (Fig.6a) and showed that the reduced TFIIH interaction was independent of its degradation (Extended data Fig.6e).

Since UVSSA plays a crucial role in the recruitment of TFIIH to lesion-stalled Pol II[7, 10], decreased UVSSA-binding likely explains the reduced TFIIH recruitment and the observed TC-NER defects. To test this, we generated *CSB* and *UVSSA* knock-in cells (Extended data Fig.7a,b), expressing mScarletI-tagged CSB and UVSSA from their endogenous locus, to allow analysis of their quantity and mobility in living cells. The mobility of these factors, as determined by FRAP, is an accurate measure for their involvement in TC-NER, as shown by their UV-induced, transcription-dependent immobilization[23, 38] (Extended data Fig.7c,d). CSB immobilization directly after UV was not affected by ELOF1 depletion, in line with our IP experiments. However, CSB remained immobilized up to 5 hours after UV (Fig.6b and Extended data Fig.7e). This prolonged binding of CSB to lesion-stalled Pol II was confirmed by IP experiments, which, additionally, showed prolonged binding of CSA (Fig.6c).

In contrast to CSB, UVSSA immobilization upon UV damage was severely reduced after ELOF1 depletion (Fig.6d, Extended data fig.7f,g), further indicating that ELOF1 plays a crucial role in the recruitment of UVSSA to lesion-stalled Pol II. UVSSA recruits the deubiquitylating enzyme USP7, which protects CSB from proteasomal degradation mediated by the ubiquitin-selective segregase VCP/p97[38, 39], which could explain the ~40% decreased CSB levels upon UV upon ELOF1 depletion (Fig.6b). Indeed, inhibition of VCP rescued CSB degradation in ELOF1-depleted cells, resulting in increased CSB immobilization upon UV (Fig.6e, Extended data Fig.7h), indicating that chromatin-bound CSB is degraded.

Recently, ubiquitylation of a single lysine in RPB1 (K1268) was described to stimulate UVSSA and TFIIH recruitment[8]. Therefore, we tested whether ELOF1 is involved in the

UV-induced Pol II ubiquitylation by studying the slower migrating ubiquitylated P-Ser2-modified RPB1 band[8]. ELOF1 KO almost completely abolished the UV-induced RPB1 ubiquitylation (Fig.6f), to the same extent as CSB KO or inhibiting NEDD8-conjugating enzyme NAE1, which controls the activity of CRL complexes[8, 9] (Extended data Fig.7i). This loss of Pol II ubiquitylation could be rescued by re-expression of Wt-ELOF1 but not by the zinc-finger mutant. Similar results were obtained using siRNA-mediated ELOF1 depletion (Extended data Fig.7j). Together, these results shows that ELOF1 is important for Pol II ubiquitylation and correct TC-NER-complex assembly upon DNA damage.

ELOF1 has an additional role outside TC-NER

Strikingly, while testing the sensitivity of ELOF1 KO, we observed that ELOF1 KO cells, but not CSB KO cells, were sensitive to the DNA crosslinker Mitomycin C (MMC) (Fig.7a). This suggests an additional function for ELOF1 in the DNA damage response, besides canonical TC-NER. The prolonged transcription block in ELOF1 KO cells upon MMC exposure (Extended data Fig.8a) suggests that this additional role for ELOF1 is linked to transcription. To confirm this additional function to TC-NER, we depleted ELOF1 in TC-NER-deficient CSB KO or NER-deficient XPA KO cells and observed an increased UV sensitivity (Fig.7b). Of note, CSB also has additional functions to ELOF1 in the response to UV-induced damage (Extended data Fig.8b). The role of ELOF1 outside TC-NER was further shown in CS patient cells characterized by inactivating mutations in CSA (CS-A), in which knockdown of ELOF1 also resulted in additional UV sensitivity (Fig.7c). As expected, knock-down of XPF induced additional UV sensitivity in CS-A cells as this also impedes GG-NER. Remarkably, this additive effect of ELOF1 is replication-dependent as it was absent in non-cycling CS-A cells (Fig.7d,e).

ELOF1 prevents transcription-mediated replication hindrance

The replication-dependent additive effect of ELOF1 to TC-NER (Fig.7), the specific role of ELOF1 in transcription (Fig.2), and prolonged Pol II stalling upon ELOF1 knockdown (Fig.5a,b), suggests that lesion-stalled Pol II collides with replication forks in the absence of ELOF1. Therefore, we investigated the impact of ELOF1 KO on DNA replication by analyzing the progression of individual replication forks. Replication fork progression was not affected upon ELOF1 KO in unperturbed conditions, indicating that ELOF1 has no role in fork progression (Fig.8a). However, 2 hours after UV, the tract length was significantly decreased in ELOF1 KO cells compared to Wt and ELOF1-complemented cells. In CSB KO cells, a small effect on fork progression was observed, however not to the same extent as in ELOF1 KO cells. This suggests that loss of the elongation factor ELOF1 results in fork progression defects upon induction of TBLs, which was also seen upon MMC-induced DNA damage (Extended data Fig.8e). This is likely due to transcription-mediated replication blockage, as the effect on replication fork progression could be inhibited by mild transcription inhibition (Fig.8b, Extended data Fig.8d) at which replication is not affected in unperturbed conditions (Extended data Fig.8d).

Transcription-replication conflicts have previously been shown to result in under-replicated DNA[2], which may cause DSBs upon mitotic progression and subsequently give rise to genome instability[40]. In line with this hypothesis, we observed a more pronounced increase

in 53BP1-foci upon UV irradiation in ELOF1 KO cells compared to Wt or CSB KO cells (Fig.8c, Extended data Fig.8f), which was observed in all stages of the cell cycle including in cells in G1 and G2 phase (Extended data Fig.8g). Furthermore, following UV we observed increased numbers of mitotic FANCD2 foci and also more mitotic DNA synthesis as visualized by EdU incorporation upon ELOF1 depletion (Fig.8d,e and extended data Fig.8h), indicative for under-replicated DNA[41, 42]. Replication-interference and under-replicated DNA are important drivers of chromosomal aberrations. In line with this, UV damage clearly resulted in an increased number of chromosomal aberrations in ELOF1 KO cells compared to Wt cells (Fig.8f).

Discussion

We unveiled an important and evolutionary conserved role for ELOF1 in the cellular response to DNA damage-induced transcription stress by two independent mechanisms: promoting TC-NER and reducing transcription-mediated replication hindrance (Fig.8g). In line with this finding, recently ELOF1 was also identified to protect to different types of TBLs in a genome-wide CRISPR screens to 27 genotoxic agents[43]. Interestingly, while the interaction of most TC-NER factors with elongating Pol II is strongly increased upon DNA damage[1, 7, 23], ELOF1 is an intrinsic part of the elongating complex in unperturbed conditions, where it stimulates transcription elongation (Fig.2). Its dual function as an elongation and repair factor can be the cause of the embryonic lethality observed in ELOF1 KO mice[44] and may explain why thus far no ELOF1 mutations were found in TC-NER-related syndromes[4].

ELOF1 promoted UVSSA-binding to lesion-stalled Pol II, resulting in subsequent TFIIH recruitment, which promotes assembly of the full incision complex to excise the TBL and restart transcription. In the absence of ELOF1, TC-NER can still be initiated since CSB and CSA are still properly recruited to lesion-stalled Pol II (Fig 6). However, UVSSA is not recruited and this suggests that more control steps are needed to recruit or stably incorporate UVSSA. This is in line with the previously observed CSA-independent UVSSA-recruitment[38, 45] and suggests that UVSSA-recruitment is not only mediated via a direct interaction with CSA[7, 46]. Such regulation of UVSSA recruitment may represent an important proof-reading step that prevents build-up of the incision complex on non-lesion stalled Pol II. An example of such a regulatory mechanism is the recently discovered TBL-induced ubiquitylation (K1268) of Pol II that is crucial for Pol II stability and TFIIH recruitment[8, 9]. Interestingly, based on recent structural analysis of the elongation complex in yeast[20], the K1268 ubiquitylation site is in close proximity of ELOF1 (Extended data Fig.9a,b). Since Pol II ubiquitylation depends on ELOF1, we hypothesize that ELOF1 might stimulate ubiquitylation by facilitating a correct orientation of the elongation complex or is involved in recruiting factors that promote Pol II ubiquitylation.

In addition to its role in TC-NER, our data show that ELOF1 plays an important role in preserving genome stability upon DNA damage, likely by preventing transcription-mediated replication stress (Fig.8). Even though CSB and ELOF1 depletion had similar effects on the prolonged binding of Pol II upon DNA damage (Fig.5a), only ELOF1 KO resulted in a clear replication defect and increased genome instability (Fig.8), suggesting that lesion-stalled Pol

II is differently processed in ELOF1-deficient cells as in CSB-deficient cells. More research is needed to fully uncover ELOF1's mechanism in preventing transcription-replication conflicts, or to test whether ELOF1 might also have transcription-independent functions affecting genome stability. Together, our results show that ELOF1 is an important guardian of elongating Pol II by protecting transcription from the severe consequences of TBLs via two mechanisms; stimulating repair and preventing transcription-replication conflicts.

Online Methods

Cell lines and cell culture

MRC-5 (SV40) immortalized human lung fibroblast cells and HCT116 colorectal cancer cells were cultured in a 1:1 mixture of DMEM (Gibco) and Ham's F10 (Invitrogen) supplemented with 10% fetal calf serum (FCS, Biowest) and 1% penicillin-streptomycin in a humidified incubator at 37°C and 5% CO_2. C5RO fibroblasts (hTert), CS3BE (CS-A, SV40), XP186LV (XP-C), CS1SP (CS-A, primary), CS216LV (CS-A, primary) cells were maintained in Ham's F10 with 15% FCS and antibiotics.

For stable isotope labeling of amino acids in culture (SILAC), cells were grown for two weeks (>10 cell doublings) in arginine/lysine-free SILAC DMEM (Thermofisher) supplemented with 15% dialyzed FCS (Gibco), 1% penicillin-streptomycin, 200 μg/ml proline (Sigma), and either 73 μg/mL light [$^{12}C_6$]-lysine and 42 μg/mL [$^{12}C_6$, $^{14}N_4$]-arginine (Sigma) or heavy [$^{13}C_6$]-lysine and [$^{13}C_6$, $^{15}N_4$]-arginine (Cambridge Isotope Laboratories).

HCT116 knock-out cells were generated by transiently transfecting HCT116 cells with a pLentiCRISPR.v2 plasmid[12] containing appropriate sgRNAs. Transfected cells were selected using 1 μg/ml puromycin (Invitrogen) for 2 days and single cells were seeded to allow expansion. Genotyping of single-cell clones was performed by immunoblotting or genomic PCR as indicated. sgRNAs sequences can be found in table 1, see below.

ELOF1 complemented cell lines were generated by lentiviral transduction in ELOF1 -/- cells. Therefore, full-length expression constructs with ELOF1-Flag-GFP, or Wt or mutated ELOF1-Flag were synthesized (Genscript). For ΔN-ELOF1-Flag, the first 15 amino acids were deleted, For Zn-ELOF1-Flag, amino acids 26 and 29 were mutated from a cysteine to a serine (TGC to TCC). Tagged ELOF1 constructs were inserted in a pLenti-CMV-puro-DEST plasmid[51]. After transduction, cells were selected with 1 μg/ml puromycin.

HCT116 osTIR1 knock-in (KI) cells[52] were generated by transiently transfecting cells with an sgRNA-containing pLentiCRISPR.v2 plasmid (sgRNA sequences in table 1, see below) targeting the stop codon of *ELOF1, CSB* or *UVSSA* and co-transfecting a homology-directed repair template, which included an Auxin-inducible Degron, fluorescent mScarletI-tag, HA-tag, hygromycin resistance cassette and homology arms (140 bp for ELOF1, 200 bp for CSB and UVSSA, sequence upon request)[53]. Subsequently, cells were seeded in a low density to allow expansion and were kept in presence of 100 μg/ml hygromycin for two weeks to select for successful recombination. Single-cell clones were genotyped and homozygous KI clones were selected for further analysis. A GFP-RPB1 KI was generated in

HCT116 Wt or ELOF1-KI cells as previously described by Steurer *et al.* [22]. MRC-5 GFP-RPB1 KI cells[22] expressing CPD-PL-mCherry were generated as described previously[21].

Genotyping PCR was performed on genomic DNA (isolated using a PureLink™ Genomic DNA Mini Kit according to manufacturer's protocol) with Phusion (NEB) or taq (Invitrogen) polymerases according to manufacturer's protocol. Primer sequences can be found in table 1, see below. If necessary for assessing genomic alterations, PCR fragments were sequenced with forward primers and indels were analyzed using TIDE analysis[54].

siRNA transfections were performed 2 or 3 days before each experiment using Lipofectamine RNAiMax (Invitrogen) according to manufacturer's protocol. siRNAs were purchased from Dharmacon: siELOF1 #1: 5'-CCGUGUGCCUAGAGGAAUUUU-3', siELOF1 #2: 5'- GAAAUCCUGUGAUGUGAAAUU-3', siCSB: 5'-GCAUGUGUCUUACGAGAUAUU-3', siXPF: M-019946-00, siSPT4: L-012602-00-0005, siSPT5: L-016234-00-0005, siCSA: L-011008-00-0005. Knock-down efficiency was determined by immunoblot or RT-qPCR.

For UV-C irradiation, cells were washed with PBS, and placed under a 254 nm germicidal UV-C lamp (Philips). Duration of irradiation was controlled with an air-pressured shutter connected to a timer and cells were irradiated with doses as indicated. Cells were treated with VCP inhibitor (Seleck Chemicals, 5 μM) directly after UV irradiation or pre-treated 1 hour before irradiation with proteasome inhibitor MG132 (Enzo, 50 μM) or NEDD8 E1 Activating Enzyme Inhibitor (NAEi) MLN4924 (R&D systems, 10 μM) where indicated. Cell were treated for 1 hour with the following chemicals: Flavopiridol (Sigma, 1 μM), THZ1 (Xcessbio, 2 μM), Mitomycin C (Sigma, 10 μg/ml unless indicated differently), or potassium bromate ($KBrO_3$, Sigma). Cells were exposed continuously to camptothecin or treated for 24 hours with cisplatin, illudin S, or hydroxyurea (all Sigma). Final concentrations of all inhibitors were diluted in culture media and cells were washed once with PBS before putting fresh media after removing damaging agent when necessary. For ionizing radiation, plates were irradiated using an RS320 X-ray cabinet (X-Strahl). For photoreactivation, cells were washed with PBS and covered with a thin layer of HBSS (Thermofisher) before exposing them to white-light tubes (General Electric Lighting Polylux LX F36W/840) for 10 minutes at 37 °C[21]. Mock-treated samples were covered with tinfoil during photo-reactivation.

GeCKO v2 lentiviral library production and transduction

We used the lentiCRISPRv2 human library designed by Shalem *et al.*[55] and obtained from Addgene. The sgRNA library was synthesized using array synthesis as previously described[55] and cloned as a pool into the lentiCRISPR transfer plasmid for virus production.

To produce the pooled lentiviral library, twelve T-225 flasks of HEK293T cells were seeded at ~40% confluency the day before transfection. Per flask 10 μg of pVSVg, and 15 μg of psPAX2 (Addgene) packaging plasmids and 20 μg of lentiCRISPR plasmid library were transfected using Lipofectamine 2000 and Plus reagent (Life Technologies), according to manufacturer's instructions. After 6 hours the medium was changed, and after 60 hours the medium was collected and centrifuged at 3,000 rpm for 10 minutes at 4 °C to pellet cell

debris. The supernatant was filtered through a 0.45 μm low protein-binding membrane (Millipore Steriflip HV/PVDF). To achieve a 300 times concentration of the GeCKO pooled library, the virus was ultracentrifuged (Sorvall) at 24,000 rpm for 2 hours at 4 °C and then resuspended overnight at 4 °C in D10 supplemented with 1% BSA. Aliquots were stored at −80°C.

Per condition 20 million MRC-5 cells were transduced at 75% confluency in 145 cm^2 dishes with concentrated lentivirus diluted in 18 ml of culture medium supplemented with 12 μg/mL polybrene (Sigma). The virus titer was determined to achieve a multiplicity of infection of <0.25. The next day, cells were re-seeded at 25% confluency in culture medium containing 2 μg/ml Puromycin. Cells were expanded for 1 week in puromycin-containing medium. Culture medium was refreshed every other day.

Genome-wide CRISPR screen

For UV irradiation or mock treatment 30 million transduced and puromycin-selected cells were seeded per condition at 40% confluency in 145 cm^2 dishes (2.25 million cells per dish) in medium without puromycin. The next day (day 0) dishes were mock-treated or irradiated with 6.8 J/m^2 UV-C. Control cells (mock-treated) and UV irradiated cells were washed with PBS and (mock) irradiated every day for 10 consecutive days. The culture medium was refreshed after each irradiation. Mock-treated cells were reseeded to 40% confluency when they reached a confluency > 90%. After the last irradiation cells were given 24 hours to recover and gDNA was isolated using the Blood & Cell Culture DNA Midi Kit (Qiagen) according the manufacturers protocol (DNA content of MRC-5 cells was estimated at 10 pg per cell, genomic DNA of max 15 million cells was loaded per column). The screen was performed in duplicate.

PCR and next-generation sequencing

Per condition, sgRNA sequences of at least 300 μg of DNA (of ~30 million cells) were amplified by PCR (PCR1) using barcoded forward primers to be able to deconvolute multiplexed samples after next-generation sequencing (primers and barcodes are listed in table 1, see below). PCR1 was performed on 3 μg of gDNA in a total volume of 50 μl per reaction. Each PCR1 reaction contained 1 U of Phusion Hot Start II Polymerase (Thermo Fisher Scientific), 1x reaction buffer, 200 nm of each dNTP, 0.5 μM of both forward and reverse primer, and 3% DMSO. The following PCR program was used: initial denaturation for 3 minutes at 98°C; 35 cycles of denaturation for 1 sec at 98°C, primer annealing for 30 sec at 60°C, extension for 30 sec at 72°C, and final extension of 10 minutes at 72°C. Individual PCR reaction products were pooled per condition and 2 μl of pooled PCR product was used for a second PCR (PCR2) using primers containing adapters for next-generation sequencing (table 1, see below). The same PCR program was used as for PCR1, except that only 15 cycles were applied. 30 μl of PCR2 product was cleaned up to remove primer pairs using the NucleoSpin Gel & PCR clean up kit (Bioké). Equal DNA content between conditions was checked by gel electrophoresis and samples were equimolarly pooled and subjected to Illumina next-generation sequencing as described before[47]. Mapped read-counts were subsequently used as input for the Model-based Analysis of Genome-wide CRISPR-Cas9 Knockout (MAGeCK) analysis software package, using version 0.5. For each

condition, two biological replicates were performed. All conditions were sequenced simultaneously. To determine which genes showed a significant negative selection after 10 days of UV treatment, the sequencing data were analyzed with the MAGeCK tool[13]. Gene ontology (GO) term enrichment analysis was performed using the g:Profiler website. Genes with a FDR<0.1 were analyzed and the top 10 biological processes affected by UV were identified.

Survival assays

For clonogenic survival assay, 200-300 cells were seeded per well in triplicate in a 6-well plate. The following day, cells were treated with different DNA damaging agents. Following treatment, colonies were grown for 7 to 10 days after which they were fixed and stained using Coomassie blue (50% methanol, 7% acetic acid and 0.1% coomassie blue (all Sigma)). To assess the growth speed of siRNA-transfected cells, 10,000 (HCT116) or 20,000 (ELOF1 -/-A) cells were seeded in a 6-well plate and grown for 10 days after transfection. Colony numbers were counted using GelCount (Oxford Optronix Ltd.). Relative colony number was plotted of at least 2 independent experiments, each performed in triplicate. Levels were normalized to mock-treated, set to 100 and plotted with SEM. Statistics was performed using independent T-test.

For AlamarBlue survival assay, siRNA-transfected cells were seeded to confluency in presence of 0.5% serum in triplicate in 96-well plates to arrest cells in $G_{0,}$ and UV-irradiated after 30 hours. 72 hours after UV irradiation, AlamarBlue® (Invitrogen) was added for 4 hours and fluorescence was measured at 570 nm using a SpectraMax iD3 reader. Data were background corrected and normalized to mock-treated conditions.

RNA isolation, cDNA synthesis and RT-qPCR

To determine ELOF1 expression levels, RNA was isolated using the RNeasy mini kit (Qiagen) and cDNA was synthesized using the SuperScript™ II Reverse Transcriptase (Invitrogen), both according to the manufacturer's protocol. The generated cDNA was amplified either by standard RT-qPCR using SYBR green or amplified performing the taqman assay and run on a CFX96 Touch™ Real-Time PCR Detection System (Biorad).

For standard RT-qPCR, PowerUp SYBR green master mix (Thermo Fisher) was used according to manufacturer's protocol. Samples were loaded in triplicate and the following program was used: 50°C for 2 min., 95°C for 2 min., 45 cycles of 15 sec. at 95°C and 1 min. at 58°C followed by a dissociation curve: 95°C for 10 sec. and heating from 65°C to 95°C with an increment of 0.5 °C, 5 sec. each. Data collection was enabled at each increment of the dissociation curve. For Taqman assay, the generated cDNA was amplified using 1x taqman assay (ELOF1: Hs00361088_g1, GAPDH: 4333764T, both Thermofisher) and 1x taqman gene expression master mix (Thermofisher) by activating UNG for 2 minutes at 50°C, activating the polymerase for 10 min. at 95°C, followed by 40 cycles of 15 seconds of denaturing at 95°C and 1 minute of annealing and extending at 60°C in a CFX96 Touch Real-Time PCR Detection System. mRNA expression levels were normalized to GAPDH using the $2^{-\Delta\Delta Ct}$ method[56].

Cell lysis and immunoblotting

Cells were directly lysed in SDS Page loading buffer (0.125M Tris pH 6.8, 2% SDS, 0.005% bromophenol blue, 21% glycerol, 4% β-mercaptoethanol) or, for assessing the chromatin fraction, one confluent 9.6 cm^2 dish was lysed for 30 minutes at 4°C in buffer containing 30 mM HEPES pH 7.5, 130 mM NaCl, 1 mM $MgCl_2$, 0.5% Triton X-100, cOmplete™ EDTA-free protease inhibitors (Roche), Phosphatase inhibitor cocktail 2 (Sigma), N-ethylmaleimide (Sigma), and 50 μM MG132i. Chromatin was pelleted at 15,000 for 10 minutes at 4°C and washed once. Finally, the chromatin was digested for 30 minutes at 4°C in presence of 50 U of benzonase (Millipore) before adding SDS Page loading buffer and incubating 5 minutes at 95°C. Chromatin fractions or cell lysates were separated on 4-15% Mini-PROTEAN TGX™ Precast Protein Gels (BioRad). Proteins were transferred onto PVDF membranes (0.45μm, Merck Millipore) at 4°C, either 1.5h at 90V with 1x transfer buffer (25mM TRIS, 190mM Glycine, 10% methanol) or overnight at 25V in 2x transfer buffer (50mM TRIS, 380mM Glycine). Membranes were blocked with 5% BSA (Sigma) in PBS-tween (0.05%) and probed with primary antibodies (Table 2, see below). Subsequently, membranes were extensively washed with PBS-tween and incubated with secondary antibodies coupled to IRDyes (LI-COR, table 3, see below) to visualize proteins using an Odyssey CLx infrared scanner (LI-COR).

Fluorescence Recovery After Photobleaching (FRAP)

For FRAP, a Leica TCS SP5 microscope (LAS AF software, Leica) equipped with a HCX PL APO CS 63x 1.40 NA oil immersion lens (ELOF1, RPB1, CSB) or Leica TCS SP8 microscope (LAS AF software, Leica) equipped with a HC PL APO CS2 63x 1.40 NA oil immersion lens (UVSSA) was used. Cells were maintained at 37°C and at 5% CO_2 during imaging. A narrow strip of 512 x 32 pixels (for ELOF1 and RPB1) or 512x16 (for CSB and UVSSA) spanning the nucleus was imaged every 400 ms (200 ms for UVSSA during pre-bleach) at 400 Hz using a 488 nm laser (RPB1) or 561 nm laser (ELOF1, CSB, UVSSA). 25 (RPB1), 40 (ELOF1), or 5 (CSB, UVSSA) frames were measured to reach steady state levels before photobleaching (1 frame 100% laser power for RPB1 and ELOF1, 2 frames for CSB and UVSSA). After photobleaching, the recovery of fluorescence was measured with 600 (ELOF1 and RPB1), 40 (CSB) or 20 (UVSSA) frames until steady-state was reached. Fluorescence intensity was measured inside and outside of the nucleus and recovery was determined by correcting for background signal and normalizing the values to the average pre-bleach fluorescence intensities. Relative fluorescence intensity levels were calculated using the pre-bleach intensities corrected for background. Immobile fractions (F_{imm}) were calculated using the individual and average (indicated by <brackets>) fluorescence intensities after bleaching (I_{bleach}) and fluorescence intensities after recovery from the bleaching ($I_{recovery}$):

$$F_{\mathrm{imm}} = 1 - (I_{recovery,UV} - \langle I_{bleach} \rangle)/(\langle I_{recovery,unc} \rangle - \langle I_{bleach} \rangle)$$

Experimental FRAP curves of Pol II were simulated using Monte-Carlo-based computational modeling as described previously[22] to determine the residence time of elongating Pol II and the fraction size of promoter-bound and elongating Pol II.

Native immunoprecipitation (IP)

Cells were mock-treated or irradiated with 16 J/m^2 UV-C 1 hour prior to cell harvest. Cell pellets were prepared from 3 confluent 145 cm^2 dishes per condition for IP followed by immunoblot or 8 confluent 145 cm^2 dishes per condition for mass spectrometry. Cells were collected by trypsinization and pelleted in cold PBS using centrifugation for 5 minutes at 1500 rpm. After one wash with cold PBS, cell pellets were stored at -80°C until immunoprecipitation.

For immunoprecipitation, pellets were thawed on ice and lysed for 20 minutes at 4°C in HEPES buffer containing 30 mM HEPES pH 7.6, 1 mM $MgCl_2$, 150 mM NaCl, 0.5% NP-40, and 1x cOmplete™ EDTA-free Protease Inhibitor Cocktail (Roche). Chromatin was pelleted by spinning 5 minutes at 10,000 g at 4°C and subsequently incubated for 1 hour at 4°C in HEPES buffer containing 500 units of Benzonase (Millipore) and 2 μg Pol II antibody (ab5095, abcam) or IgG (sc2027, Santacruz) to digest the chromatin. After 1 hour, the NaCl was increased to 300 mM to inactivate benzonase and antibody-binding was continued for another 30 minutes. The undigested fraction was pelleted at 13,200 rpm for 10 minutes at 4°C and the soluble, antibody-bound fraction was immunoprecipitated for 90 minutes at 4°C using 25 μL slurry salmon sperm protein A agarose beads (Millipore). Unbound proteins were removed by washing the beads 5 times in wash buffer (30 mM HEPES pH 7.6, 150 mM NaCl, 1mM EDTA, 0.5% NP-40, and 0.2x cOmplete™ EDTA-free Protease Inhibitor Cocktail). Bound proteins were eluted in SDS page loading buffer and separated on 4-15% Mini-PROTEAN TGX™ Precast Protein Gels (BioRad). Samples were processed for immunoblotting or fixed and stained for mass spectrometry using Imperial protein stain (Pierce) according to manufacturer's protocol.

For ELOF1 IP, the same protocol was followed but instead of adding antibody during chromatin digestion, precipitation was performed using RFP-Trap® agarose beads (Chromotek) and binding control agarose beads (Chromotek).

Cross-linked immunoprecipitation

Cells were mock-treated or irradiated with 16 J/m^2 UV-C one hour prior to cell harvest. Cell pellets were prepared from 8 confluent 145 cm^2 dishes per condition for mass spectrometry. MRC-5 GFP-RPB1 KI cells were used for Pol II IP (Flag-beads) and HCT116 ELOF1-KI cells were used for ELOF1 IP (HA-beads).

Crosslinked IP was performed as described previously[45] with modifications as indicated. Cells were cross-linked with 1% paraformaldehyde (PFA) in serum-free DMEM for 7 minutes with constant shaking before quenching the reaction for 5 minutes with glycine (final concentration of 0.125 M). Cells were collected by scraping in PBS with 10% glycerol and 1 mM PMSF and pelleted for 15 minutes at maximum speed at 4°C. Consequently, chromatin was purified by washing the cell pellets for 30 minutes at 4°C in buffer 1 (50 mM HEPES, 150 mM NaCl, 1 mM EDTA, 0.5 mM EGTA, 0.25% Trition X-100, 0.5% NP-40, 10% glycerol), pelleting the cells 10 minutes at 1300 rpm, washing the pellet twice with buffer 2 (10 mM Tris pH 8.0, 200 mM NaCl, 1 mM EDTA, 0.5 mM EGTA) and finally pelleting the chromatin, all at 4°C. Chromatin was sonicated in RIPA buffer (10 mM Tris pH

7.5, 150 mM NaCl, 5 mM EDTA, 0.1% SDS, 1% Sodium Deoxycholate and 0.5 mM EGTA) using the Bioruptor Sonicator (Diagenode) with 14 cycles of 15s on/15s off using the highest amplitude. Extracted chromatin was collected by spinning 15 minutes at maximum speed and pre-cleared for 30 minutes with Protein G agarose beads (Pierce) at 4°C. IP was performed by incubating 4 hours at 4°C with Flag M2 agarose beads (Sigma). Finally, aspecific interactors were removed by washing five times with RIPA buffer and proteins were eluted and crosslinking was reversed by incubating 30 minutes at 95°C in SDS Page loading buffer. Samples were separated on 4-15% Mini-PROTEAN TGX™ Precast Protein Gels (BioRad) and fixed and stained using imperial protein stain in preparation of mass spectrometry. To all buffers, 1 mM PMSF, 0.5 mM Na_2VO_4, 5 mM NaF, 5 mM NaPPi, 10 mM β-glycerol and cOmplete™ EDTA-free Protease Inhibitor Cocktail were added.

For ELOF1 IP, the same protocol was followed with minor alterations. Cells were crosslinked in 1 mM dithiobis(succinimidyl propionate) (DSP) in PBS for 30 minutes and quenched by adding Tris pH 7.5 to a final concentration of 25 mM for 10 minutes. IP was performed using HA-agarose beads (Sigma) and beads were incubated for 5 minutes at 95°C to elute and reverse cross-linked immunocomplexes.

Mass spectrometry

SDS-PAGE gel lanes were cut into slices and subjected to in-gel reduction with dithiothreitol (Sigma, D8255), alkylation with iodoacetamide (Sigma, I6125) and digestion with trypsin (sequencing grade; Promega) as previously described[38]. Nanoflow liquid chromatography tandem mass spectrometry (nLC-MS/MS) was performed on an EASY-nLC 1200 coupled to a Lumos Tribid Orbitrap mass spectrometer (ThermoFisher Scientific) operating in positive mode. Peptide mixtures were trapped on a 2 cm x 100 μm Pepmap C18 column (Thermo Fisher 164564) and then separated on an in-house packed 50 cm x 75 μm capillary column with 1.9 μm Reprosil-Pur C18 beads (Dr. Maisch) at a flowrate of 250 nL/min, using a linear gradient of 0–32% acetonitrile (in 0.1% formic acid) during 90min. The eluate was directly sprayed into the electrospray ionization (ESI) source of the mass spectrometer. Spectra were acquired in continuum mode; fragmentation of the peptides was performed in data-dependent mode by HCD. Mass spectrometry data were analyzed using the MaxQuant software (version 1.6.3.3). The false discovery rate (FDR) of both PSM and protein was set to 0.01 and the minimum ratio count was set to 1. The Andromeda search engine was used to search the MS/MS spectra against the UniProt database (taxonomy: Homo sapiens, release June 2017), concatenated with the reversed versions of all sequences. A maximum of two missed cleavages was allowed. In case the identified peptides of two proteins were the same or the identified peptides of one protein included all peptides of another protein, these proteins were combined by MaxQuant and reported as one protein group. Before further analysis, known contaminants and reverse hits were removed. Gene ontology (GO) term enrichment analysis was performed using the g:Profiler website. Genes with an average SILAC ratio of >2.5 were analyzed and the top 10 biological processes affected by UV were identified.

DRB/TT$_{chem}$-seq method

The DRB/TT$_{chem}$-seq was carried out as described in Gregersen *et al.* [24] in two biological replicates. Briefly, 8 × 10^6 cells were incubated in 100 μM DRB (Sigma-Aldrich) for 3.5 hours. The cells were then washed twice in PBS and fresh, DRB-free medium was added to restart transcription. The RNA was labelled *in vivo* with 1 mM 4SU (Glentham Life Sciences) for 10 minutes prior to the addition of TRIzol (Thermo Fisher Scientific), which was used to stop the reaction at the desired time point. Following extraction, 100 μg of RNA was spiked-in with 1 μg 4-thiouracile labelled S. cerevisiae RNA (strain BY4741, MATa, his3D1, leu2D0, met15D0, ura3D0), and then fragmented with NaOH and biotinylated with MTSEA biotin-XXlinker (Biotium). The biotinylated RNA was then purified using μMACS Streptavidine MicroBeads (Miltenyi Biotec) and used for library preparation. The libraries were amplified using the KAPA RNA HyperPrep kit (Roche) with modifications as described in[9].The fragmentation step was omitted and the RNA, resuspended in FPE Buffer, was denatured at 65°C for 5 min. Two SPRI bead purifications were carried out, with a bead-to-sample volume ratio of 0.95x and 1x, respectively. The libraries were then sequenced with single end 75bp reads on the Hiseq4000, with ~50,000,000 reads per sample.

Computational Analysis

DRB/TT$_{chem}$-seq data were processed using previously published protocol[24]. Briefly, reads were aligned to human GRCh38 Ensembl 86. Read depth coverage was normalized to account for differences between samples using a scale factor derived from a yeast spike-in aligned and counted against Saccharomyces cerevisiae R64-1-1 Ensembl 86.[57]Biological replicate alignments were combined for the purpose of visualization and wave-peak analysis in order to increase read-depth coverage.

A set of non-overlapping protein-coding genes of>200kb and of 50-100 kb were selected for wave-peak analysis. A meta-gene profile was calculated by taking a trimmed mean of each basepairs coverage in the region -2kb:+200kb around the TSS. This was further smoothened using a spline. Wave peaks were called at the maximum points on the spline, with the stipulation that the peak must advance with time before being subjected to manual review. Elongation rates (kb/min) were calculated by fitting a linear model to the wave peak positions as a function of time.

EU incorporation

Cells were grown on coverslips and transcription levels were measured by pulse labeling with 5'ethynyl uridine (EU, Jena Bioscience) in Ham's F10 medium supplemented with 10% dialyzed FCS and 20 mM HEPES buffer (both Gibco). Cells were labeled for 30 minutes using 400 μM EU (MRC-5 cells) or for 1 hour with 200 μM EU (HCT116 cells) before fixation with 3.7% formaldehyde (FA, Sigma) in PBS for 15 minutes at room temperature (RT). After permeabilisation with 0.1% Triton X-100 in PBS for 10 minutes and blocking in 1.5% BSA in PBS for 10 minutes, Click-it chemistry-based azide coupling was performed by incubation for 1 hour with 60 μM Atto594 Azide (Attotec, Germany) in 50 mM Tris buffer (pH 8) with 4 mM $CuSO_4$ (Sigma), and 10 mM freshly prepared ascorbic acid (Sigma). DAPI (Brunschwieg Chemie) was added to visualize the nuclei. Coverslips

were washed with 0.1% Triton in PBS and PBS only and mounted with Aqua-Poly/Mount (Polysciences). Cells were imaged with a Zeiss LSM 700 Axio Imager Z2 upright microscope equipped with a 40x Plan-apochromat 1.3 NA oil immersion lens or 63x Plan-apochromat 1.4 NA oil immersion lens (Carl Zeiss Micro Imaging Inc.). Integrated density of the EU signal in the nuclei was quantified using ImageJ. Therefore, the surface of each nucleus was determined based on the DAPI signal and mean fluorescence intensity was determined, corrected for the background signal. With these values, the integrated density was calculated, and plotted as single cell point with the average and SEM.

For assessing recovery of transcription after UV, cells were mock-treated or irradiated with 8 J/m^2 UV-C 2 or 18 hours before EU incorporation. For recovery after mitomycin C, cells were mock-treated or incubated for 2 hours with 10 μg/ml Mitomycin C followed by a recovery period of 2 or 22 hours in normal medium. Integrated density was normalized to mock-treated.

TC-NER-specific UDS

Amplified UDS was performed as described previously[27]. Briefly, siRNA transfected primary XP186LV (XP-C patient cells) were serum-deprived for at least 24 hours in Ham's F10 (Lonza) containing 0.5% FCS and antibiotics to arrest cells in G_0. Cells were irradiated using 8 J/m^2 UV and labelled for 7 hours with 20 μM 5-Ethynyl-2'-deoxyuridin (EdU) and 1 μM Floxouridine (Sigma). Subsequently, a 15-minute chase was performed with normal medium (0.5% FCS) supplemented with 10 μM thymidine (Sigma) to remove unincorporated EdU and cells were fixed and permeabilized with 3.7% FA and 0.5% Triton X-100 for 15 minutes. After permeabilizing the cells for 20 minutes with 0.5% Trition in PBS and washing with 3% BSA in PBS, endogenous peroxidase activity was quenched using 2% hydrogen peroxide (Sigma) for 15 minutes and incubated with PBS+ (0.5% BSA + 0.15 % glycine). Click-it chemistry was performed using the Click-it reaction cocktail containing Azide-PEG3-Biotin Conjugate (20 μM, Jena Bioscience), 1× Click-it reaction buffer (ThermoFisher Scientific), copper(III) sulfate (0.1 M) and 10× reaction buffer additive (ThermoFisher Scientific) for 1 hour and washed with PBS. To amplify the signal, coverslips were incubated for 1 hour using HRP-streptavidin conjugate (500 μg/ml), followed by PBS washes and a 10-minute incubation with Alexa-Fluor 488 labeled tyramide (100x stock, Thermofisher Scientific). Coverslips were washed with PBS and PBS+ and the nuclei were stained with DAPI in 0.1% triton. DAPI was washed away with 0.1% triton and slides were mounted using Aqua-Poly/Mount.

Unscheduled DNA Synthesis (UDS)

Cells were grown to confluency on coverslips and serum-deprived (0.5%) for 2 days to arrest cells in G_0. Cells were irradiated with 16 J/m^2 and labeled with 20 μM EdU (Invitrogen) in Ham's F10 supplemented with 10% dialyzed FCS and 20 mM HEPES buffer (both Gibco) for 3 hours before fixation for 15 minutes (3.7% FA and 0.5% triton X-100). Background signal was blocked by washing twice with 3% BSA in PBS for 10 minutes and nuclei were permeabilized for 20 minutes using 0.5% triton in PBS. EdU incorporation was visualized using Click-it chemistry, imaged and analyzed as described in the section *EU incorporation* with the adjustment that click-it reaction was performed for 30 minutes.

Yeast strains

Yeast deletion strains used in this study are derivatives of the wild type strain BY4741 (*MATa his3Δ1 leu2Δ0 met15Δ0 ura3Δ0*) and Y452 (*MATα, ura3-52, his3–1, leu2-3, leu2-112, cir°*). The gene deletions were made by transformation of yeast cells with PCR products bracketing selection markers[58] or following published methods[59].

Yeast UV sensitivity assay

Yeast cells were grown in YPD medium to mid-log phase. For spotting assay, cells were serially 10-fold diluted in fresh YPD medium and spotted on YPD plates. After exposure to different doses of UV-C light (254 nm), plates were incubated at 30°C in the dark and images were taken after 3-5 days of incubation. For quantitative UV survival assay, diluted yeast cells were plated on YPD plates and exposed to the indicated UV doses. The number of colonies on each plate was counted after incubating for 3 days at 30°C in the dark.

CPD-seq library preparation and sequencing

CPD-seq analysis of repair in Wt and *elf1*Δ mutant strains was performed as previously described[33]. Briefly, yeast cells were grown to mid-log phase, pelleted, re-suspended in dH_2O, and irradiated with 125 J/m^2 UV-C light (254 nm). After UV treatment, cells were incubated in the dark in pre-warmed, fresh YPD medium for repair. Cells were collected before UV irradiation (No UV), immediately after UV (0 hours), and following a 2-hour repair incubation. The cells were pelleted and stored at -80°C until genomic DNA isolation.

Genomic DNA extraction, CPD-seq library preparation and quality control, sequencing with an Ion Proton sequencer, and data processing were performed as previously described[33]. The resulting sequencing reads were aligned to the yeast genome (saccer3) using Bowtie 2[60]. Only CPD-seq reads associated with lesions at dipyrimidine sequences (i.e., TT, TC, CT, CC) were retained for further analysis.

Bin analysis for CPD repair along the transcribed strand (TS) and non-transcribed strand (NTS) of ~5000 yeast genes was performed as previously described[61], using transcription start site (TSS) and polyadenylation site (PAS, also referred to as transcription termination site, TTS) coordinates from Park *et al.* [62]. A similar gene bin analysis was displayed for each yeast gene using the Java Treeview program[63, 64]. Genes were sorted according to transcription rate, which was obtained from a published gene expression database of transcription frequencies for wild-type yeast[65]. Single nucleotide resolution repair analysis adjacent to the TSS was performed as previously described[61, 66]. Nucleosome dyad coverage from MNase-seq experiments were obtained from Weiner *et al.*,[50] as reference. CPD-seq data for *elf1Δ* and Wt yeast was normalized using the fraction of CPDs remaining determined for bulk genomic DNA by T4 endonuclease V digestion and alkaline gel electrophoresis (see below).

Analysis of bulk CPD repair in UV irradiated yeast

Alkaline gel electrophoresis to assay global DNA repair of bulk DNA was conducted as previously described[67]. Yeast cell cultures were grown to mid-log phase in YPD media. Yeast cell cultures were briefly centrifuged to pellet, resuspended in dH_2O, and exposed to

100 J/m^2 UV-C light or left unirradiated for the “No UV” sample. Following irradiation, yeast cells were resuspended in YPD and incubated at 30˚C. Aliquots were taken at each repair time point, briefly centrifuging to discard media supernatant prior to storing yeast cells at -80˚C. Genomic DNA was isolated by bead beating the yeast cell pellets in 250 μL lysis buffer (2% Triton-X 100, 1% SDS, 100 mM NaCl, 10 mM Tris-Cl pH 8, 1 mM Na_2EDTA) and 300 μL Phenol-Chloroform-Isoamyl alcohol (25:24:1). 300 μL TE pH 8 was added to each tube, briefly vortexing to mix. Samples were centrifuged and the DNA-containing aqueous layer was transferred to a fresh tube for ethanol precipitation. DNA pellets were resuspended in TE pH 8 containing 0.2 mg/mL RNase A, incubating at 37˚C for 15 minutes prior to enzymatic digestion. Equal amounts of DNA were then treated with T4 endonuclease V (T4 PDG; NEB) and resolved by electrophoresis on a 1.2% alkaline agarose gel. Following neutralization and staining with SYBR Gold (Invitrogen), alkaline gels were imaged using the Typhoon FLA 7000 (GE Healthcare) and analyzed using ImageQuant TL 8.2 (GE Healthcare). The number of CPD lesions per kb was estimated using the ensemble average pixel density of each lane, corrected by the no enzyme control lane. Percent repair was calculated by normalizing the number of CPDs per kb to the no repair time point. Graphs represent the mean and SEM of at least 3 independent experiments.

Repair analysis of UV induced CPDs in *RPB2* locus

Yeast cells were grown in synthetic dextrose (SD) medium at 30°C to late log phase ($A_{600} \approx$ 1.0), irradiated with 120 J/m^2 of UV-C and incubated in YPD medium at 30°C in the dark. At different times of the repair incubation, aliquots were removed, and the genomic DNA was isolated. To map the induction and repair of UV-induced CPDs at the nucleotide resolution in a specific gene, libraries of DNA fragments adjoining the lesions were created by using the LAF-Seq (Lesion-Adjoining Fragment Sequencing) strategy[68] with some modifications. Briefly, the isolated genomic DNA was restricted with HincII and NruI to release a 553 bp *RPB2* gene fragment (168 bp upstream and 385 bp downstream of the transcription start site) and incised at the CPDs with T4 endonuclease V and treated *E. coli* endonuclease IV (New England Biolabs). The 3’ ends of the restricted and CPD-incised DNA fragments were ligated to Illumina sequencing adapters by using Circligase (Lucigen). After PCR amplification, the libraries were sequenced by using an Illumina HiSeq platform.

The sequencing reads were aligned to the *RPB2* gene by using Bowtie 2[60]. The numbers of reads from the UV-irradiated samples were normalized to those from the control (unirradiated) samples. Reads corresponding to CPDs at individual sites along the *RPB2* gene fragment were counted after subtraction of the background counts (in the unirradiated samples) by using codes in R. To more directly ‘visualize’ the CPD induction and repair profiles, images with band intensities corresponding to counts of aligned sequencing reads were created by using codes in R and MATLAB.

C. elegans strains and UV sensitivity assays

C. elegans strains were cultured according to standard methods and outcrossed against Bristol N2, which was used as wild type. Mutant alleles were *xpc-1(tm3886)*, *csb-1(ok2335)*, and *elof-1(emc203)*. The loss of function *elof-1(emc203)* (Extended data Fig.6i) mutant strain was generated by injection of Cas9 protein together with tracrRNA and

two crRNAs targeting *elof-1* (CAGTTGAATTGGGTGTCGAG and AGACGTCGATTGGCTCGGAG; Integrated DNA Technologies). Deletion animals were selected by genotyping PCR and sequencing. UV survival experiments were performed as described previously[36]. Animals were irradiated at the indicated dose using two Philips TL-12 (40W) tubes emitting UV-B light. Briefly, 'germ cell and embryo UV survival' was determined by allowing UV-irradiated staged young adults to lay eggs on plates for 3 hours. To calculate the survival percentage, the total number of hatched and unhatched eggs was counted after 24 hours. For the 'L1 larvae UV survival', staged L1 larvae were UV irradiated and grown for 48 hours. Survival percentage was calculated by counting surviving animals that developed beyond the L2 stage and arrested animals as L1/L2 larvae.

Metaphase spreads and chromosomal aberrations

Metaphase spreads were carried out as described previously[69]. Briefly, cells were irradiated with 4 J/m^2 or mock-treated 48 or 72 hours before preparing metaphase spreads (final confluence of 50-80%). Cells were arrested at metaphase by incubating with colcemid (*N*-methyl-*N*-deacetyl-colchicine, Roche, **10295892001**) for the last 14 hours before harvesting the cells. Collected cells were treated with hypotonic solution (KCl 0.075 M) for 30 minutes at 37°C and fixed with methanol:acetic acid 3:1. Telomere-FISH was further carried out to study chromosomal aberrations. Metaphases were hybridized with telomere-repeat specific peptide nucleic acid (PNA) probes (Applied Biosystems) as described to label telomeres[70]. A minimum 60 metaphase images were obtained using Carl Zeiss Axio Imager D2 microscope using 63x Plan Apo 1.4 NA oil immersion objective and analyzed with ImageJ software for chromosomal aberrations.

DNA fiber analysis

DNA fiber analysis was carried out as described previously[69, 71]. Briefly, cells were sequentially pulse-labeled with 30μM CldU (c6891, Sigma-Aldrich) and 250μM IdU (I0050000, European Pharmacopoeia) for 15min. For assessing fork progression after DNA damage, cells were irradiated with 4 J/m^2 UV and incubated for 2 hours before pulse-labeling. After labeling, cells were collected and resuspended in PBS at 2.5×10^5 cells per ml. The labeled cells were mixed 1:1 with unlabeled cells, and 2.5μl of cells was added to 7.5μl of lysis buffer (200mM Tris-HCl, pH 7.5, 50mM EDTA, and 0.5% (w/v) SDS) on a glass slide. After 8min, the slides were tilted at 15–45°, and the resulting DNA spreads were air dried, fixed in 3:1 methanol/acetic acid overnight at 4°C. The fibers were denatured with 2.5M HCl for 1hour, washed with PBS and blocked with 0.2% Tween-20 in 1% BSA/PBS for 40min. The newly replicated CldU and IdU tracks were incubated (for 2.5hours in the dark, at RT with anti-BrdU antibodies recognizing CldU and IdU (Table 2, see below), followed by a 1-hour incubation with secondary antibodies at RT in the dark: anti–mouse Alexa Fluor 488 and anti–rat Cy3 (Table 3, see below). Fibers were visualized and imaged by Carl Zeiss Axio Imager D2 microscope using 63X Plan Apo 1.4 NA oil immersion objective. Data analysis was carried out with ImageJ software. A one-way ANOVA was applied for statistical analysis using the GraphPad Prism Software.

Immunofluorescence

Immunofluorescence was carried out as described previously[72]. Cells were grown on 24-mm glass coverslips and mock-treated or irradiated with 8 J/m^2 48, 24 or 6 hours prior to fixation for 15 minutes in PBS with 3.7% FA. Subsequently, cells were permeabilized with 0.1% Triton X-100 in PBS and washed with PBS+ (0.15% BSA and 0.15% glycine in PBS). Cells were incubated for 2 hours at RT with rabbit anti-53BP1 antibody (table 2, see below) in PBS+. Thereafter, cells were washed with PBS+, 0.1% Triton and PBS+ before incubating 2 hours at RT with donkey anti-rabbit Alexa Fluor 594 conjugated antibody (table 3, see below) and DAPI. After washes with PBS+ and 0.1% Triton, coverslips were mounted with Aqua-Poly/Mount. Images were acquired with a Zeiss LSM700 Axio Imager Z2 upright microscope equipped with a 63x Plan-apochromat 1.4 NA oil immersion lens (Carl Zeiss Micro Imaging Inc.). Number of foci per nucleus was counted by using ImageJ.

Mitotic FANCD2 and EdU foci

HCT116 or RPE-1 *TP53*$^{-/-}$ cells were seeded on glass coverslips in 6-well plates. If indicated, RPE-1 *TP53*$^{-/-}$ cells were transfected with siRNAs for 24 hours, after which the cells were irradiated with 4J/m^2 UV 254 nm using a Stratalinker (Stratagene, US) and left for 48 hours. RPE-1 *TP53*$^{-/-}$ cells were synchronized at the G2/M border using a 4-hour incubation with the CDK1 inhibitor RO-3306 (final concentration 5 μM, Axon Medchem, Groningen, #1530) treatment, and released into pro/prometaphase while pulsed with EdU (20 μM) for 30 minutes. HCT116 cells were irradiated with 4J/m^2 UV at 24 hours after seeding, and were left for 48 hours. When indicated, cells were pulsed for 30 minutes with 20 μM EdU. Cells were fixed using 2% formaldehyde with 0.1% Triton-X-100 in PBS for 30 minutes, and were subsequently permeabilized for 10 minutes in PBS with 0.5% Triton X-100. Cells were than stained with anti-FANCD2 (Novusbio, NB100-182) and Alexa-488 or Alexa-647-conjugated secondary antibodies, and counterstained with DAPI (Sigma). The EdU Click-chemistry reaction was performed as per instructions of the manufacturer (Click-iT™ EdU Cell Proliferation Kit for Imaging, Alexa Fluor™ 647, Thermofisher Scientific).

Statistics and reproducibility

Experimental data was plotted and analyzed using GraphPad Prism 9.0.1 (GraphPad Software Inc.) built-in tests, and are indicated in the figure legends, unless otherwise indicated. The number of samples analyzed per experiment are reported in the respective figure legends. All experiments were independently repeated at least two times with similar results obtained.

Europe PMC Funders Author Manuscripts

Extended Data

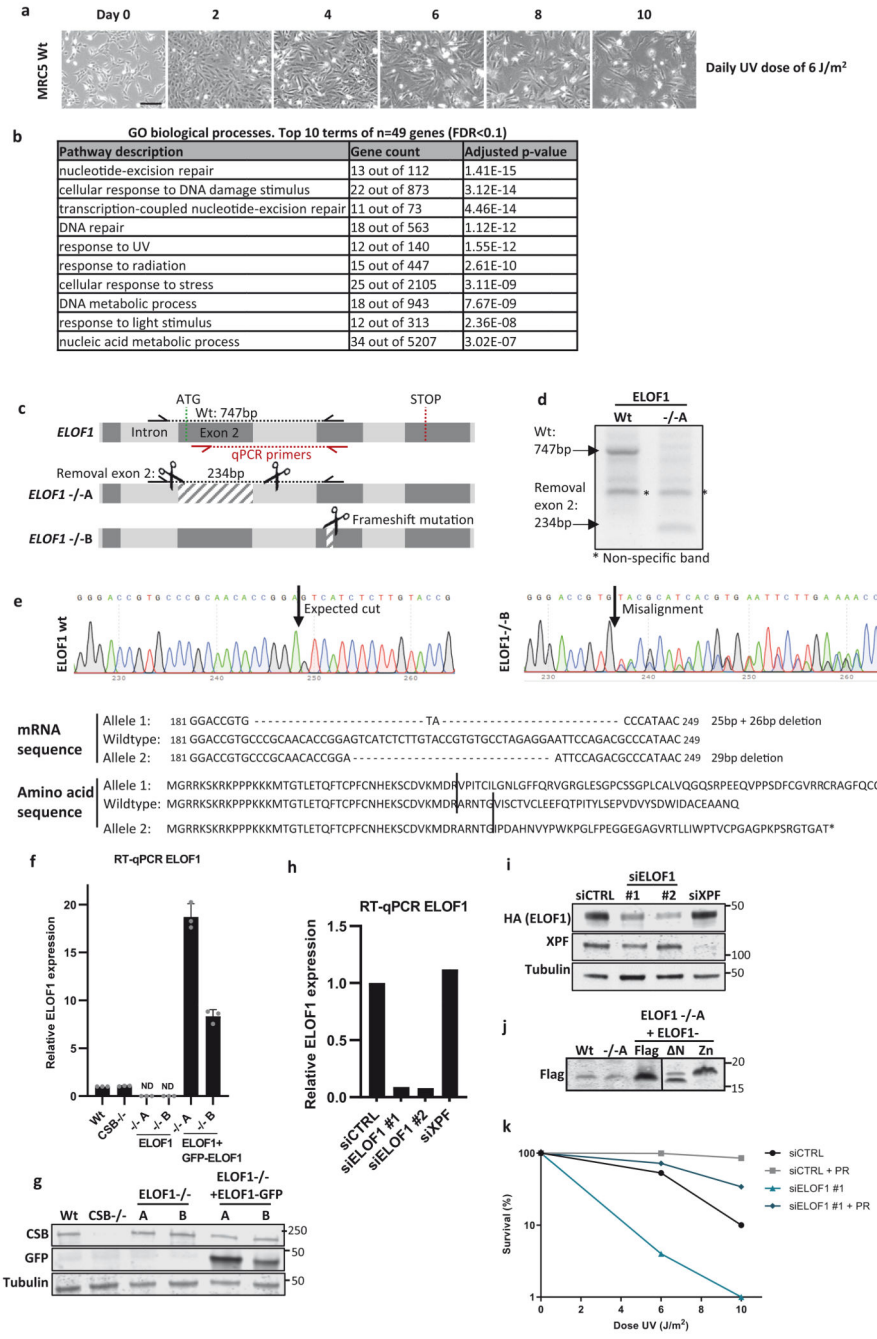

Extended Data Fig. 1. Generation of ELOF1 knock-in and out cells

(a) Brightfield images of MRC-5 cells irradiated with indicated doses of UV-C for 10 consecutive days. Images were taken every other day. Scale bar: 60 μm. **(b)** Top 10 enriched GO terms (biological process) identified using g:Profiler of UV-sensitive genes with FDR<0.1 (n=49). **(c)** Schematic of the genomic *ELOF1* locus. Scissors indicate target regions of the sgRNAs used to generated *ELOF1* KO (-/-) cells, half arrows indicate primers

used for genotyping as shown in (c). Red arrows indicate location of the qPCR primers as shown in (e). **(d+e)** Genotyping of ELOF1 KO (-/-) cells, both originating from a single cell clone. **(d)** Genotyping PCR of loss of exon 2 in *ELOF1* -/-A cells. Assays in d, i, j and g have been performed two times with similar results. **(e)** Top panel: Sequencing results showing frameshift mutations in the targeted genomic locus of *ELOF1* -/-B. Bottom panel: Amino acid sequence of ELOF1 in ELOF1 -/-B cells. **(f)** Relative ELOF1 levels in indicated HCT116 Wt and ELOF1 KO (-/-) cells, with ELOF1 re-expression where indicated, as determined by RT-qPCR. Relative ELOF1 mRNA expression was normalized to GAPDH signal and levels in Wt cells were set to 1. ND=not detected. Data shown in represent average ± SEM (n=3 independent experiments. **(g)** Immunoblot of indicated HCT116 cell lines showing CSB or ELOF1-GFP expression. Tubulin was used as loading control. **(h)** Relative ELOF1 levels in HCT116 cells transfected with indicated siRNAs as determined by RT-qPCR. Relative ELOF1 expression was normalized to GAPDH signal and siCTRL levels were set to 1. Data shown represent average from 2 independent experiments. **(i)** Immunoblot showing endogenous ELOF1 and XPF levels in *ELOF1-mScarletI-HA* KI cells (Extended data fig. 2a) transfected with indicated siRNAs. Tubulin was used as loading control. **(j)** Immunoblot showing expression of Flag-tagged Wt or indicated ELOF1 mutants in HCT116 ELOF1 -/-A cells. **(k)** Relative colony survival of CPD photolyase cells transfected with indicated siRNAs. PR indicates CPD removal by photoreactivation. Plotted curves represent averages of 2 independent experiments. Numerical data and uncropped blots are provided in source data extended data fig. 1.

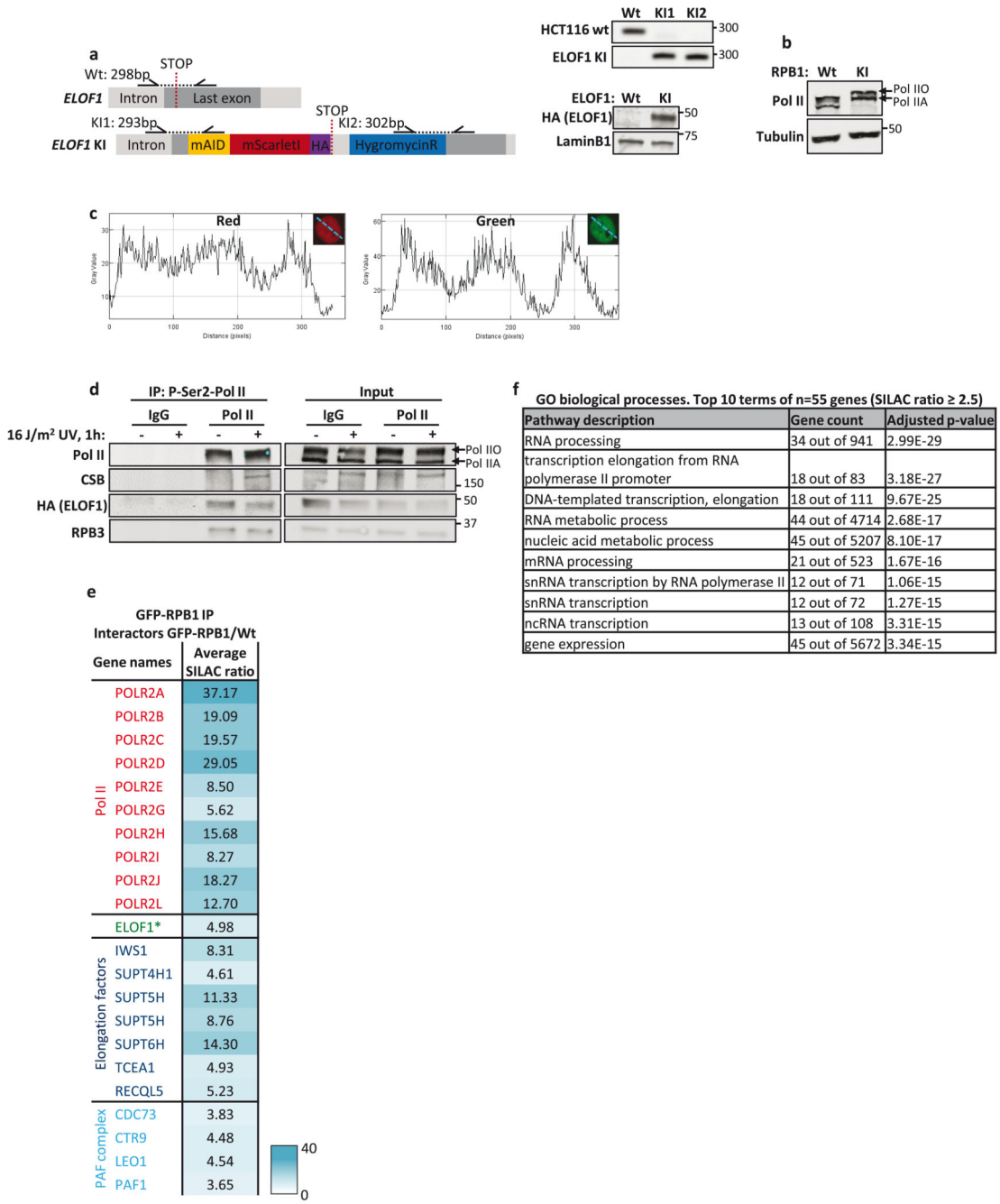

Extended Data Fig. 2. ELOF1 is part of the Pol II complex.

(a) Left panel: Schematic of the genomic locus of *ELOF1* for generating *ELOF1-mScarletI-HA* KI cell line. Half arrows indicate primer locations. Right panel: Genotyping PCR and immunoblot for *ELOF1*-KI cell line (top). LaminB1 was used as loading control (bottom). **(b)** Immunoblot of HCT116 *GFP-RPB1* KI. Tubulin was used as loading control. Immunoblots have been performed two times with similar results. **(c)** Histograms showing intensities of GFP and mScarletI measured over the indicated dotted line in HCT116 double KI cells. **(d)** Native immunoprecipitation of P-Ser2-modified Pol II in HCT116 cells

followed by immunoblotting for indicated proteins. Cells were harvested 1 hour after mock treated or irradiation with 16 J/m^2 UV-C. IgG was used as binding control. IP has been performed two times with similar results. **(e)** Interaction heat map based on the SILAC ratios of MRC-5 GFP-RPB1-interacting proteins as determined by quantitative interaction proteomics. Average SILAC ratios of duplicate experiments are plotted and represent RPB1-interactors relative to empty beads. SILAC ratio >1 indicates increase in interaction. * indicates proteins quantified in one experiment. **(f)** Top 10 enriched GO terms (biological processes) identified using g:Profiler of 55 proteins identified as ELOF1 interactor with an average SILAC ratio of 2.5 or higher. Uncropped blots are provided in source data extended data fig. 2.

Europe PMC Funders Author Manuscripts

Europe PMC Funders Author Manuscripts

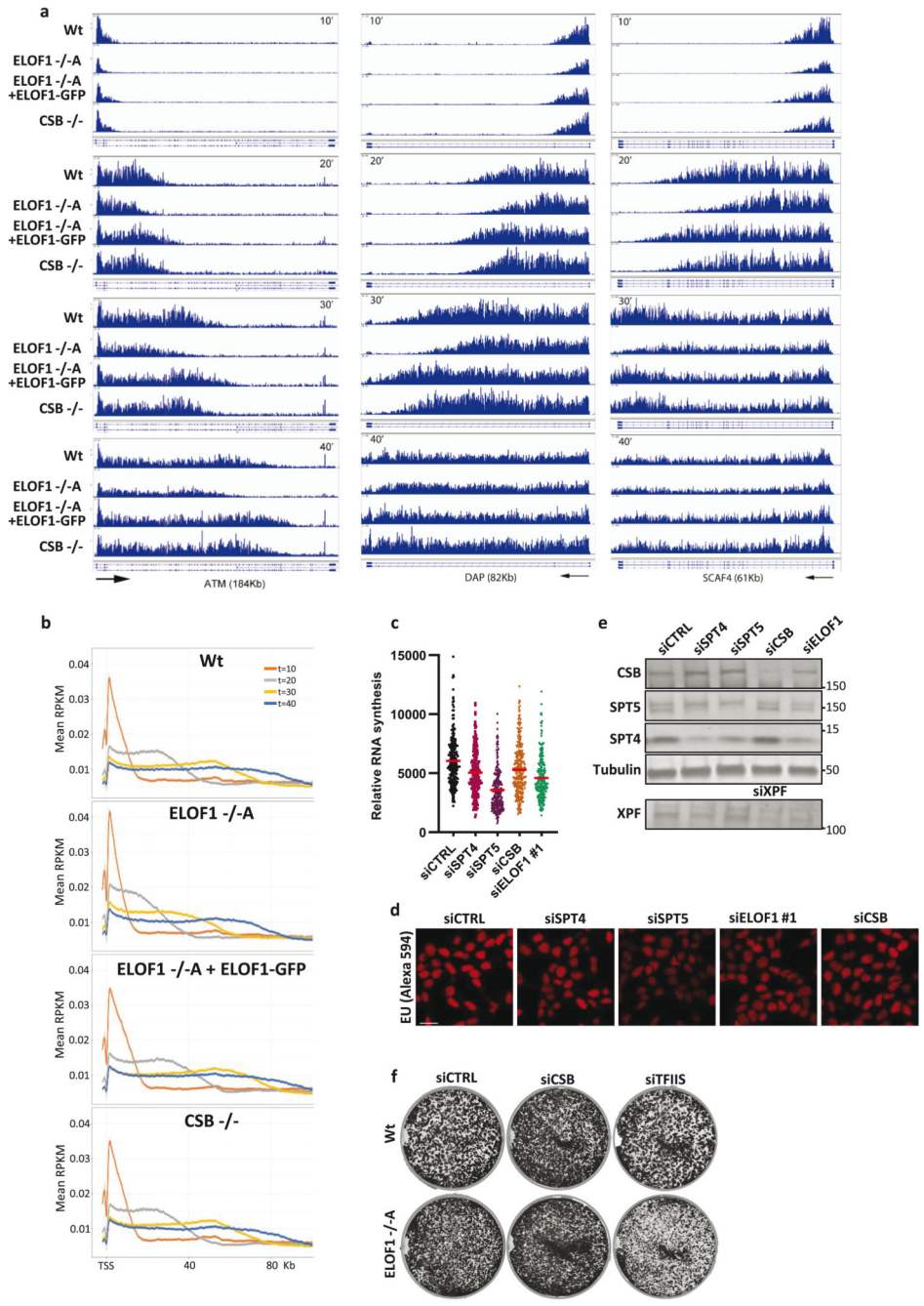

Extended Data Fig. 3. ELOF1 stimulates transcription elongation.

(a) Browser tracks from DRB/TT_{chem}-seq experiment at *ATM, DAP* and *SCAF4*. Results are shown 10, 20, 30 or 40 minutes after DRB release. **(b)** Metagene profiles of DRB/TT_{chem}-seq in HCT116 Wt or indicated KO (-/-) cells, with ELOF1 re-expression where indicated, 10, 20, 30, or 40 minutes after DRB release for 50-100Kb long genes. **(c)** Transcription levels as determined by relative EU incorporation in HCT116 cells transfected with indicated siRNAs. Red lines indicate average integrated density ± SEM. siCTRL n=247, siSPT4 n=272, siSPT5 n=288, siCSB n=286, siELOF1 #1 n=285 cells analyzed

across 3 (siELOF1 and siCSB) and 4 (siCTRL) independent experiments. **(d)** Representative images of EU incorporation in HCT116 cells transfected with indicated siRNAs. Scale bar: 20 μm. **(e)** Immunoblot for indicated proteins in HCT116 cells transfected with indicated siRNAs. Tubulin was used as loading control. Experiment has has been performed two times with similar results. **(f)** Images of HCT116 Wt and ELOF1 -/-A cells transfected with indicated siRNAs, stained with coomassie blue 10 days after transfection. Cell growth experiment has been executed two times with similar results. Numerical data and uncropped blots are provided in source data extended data fig. 3.

Europe PMC Funders Author Manuscripts

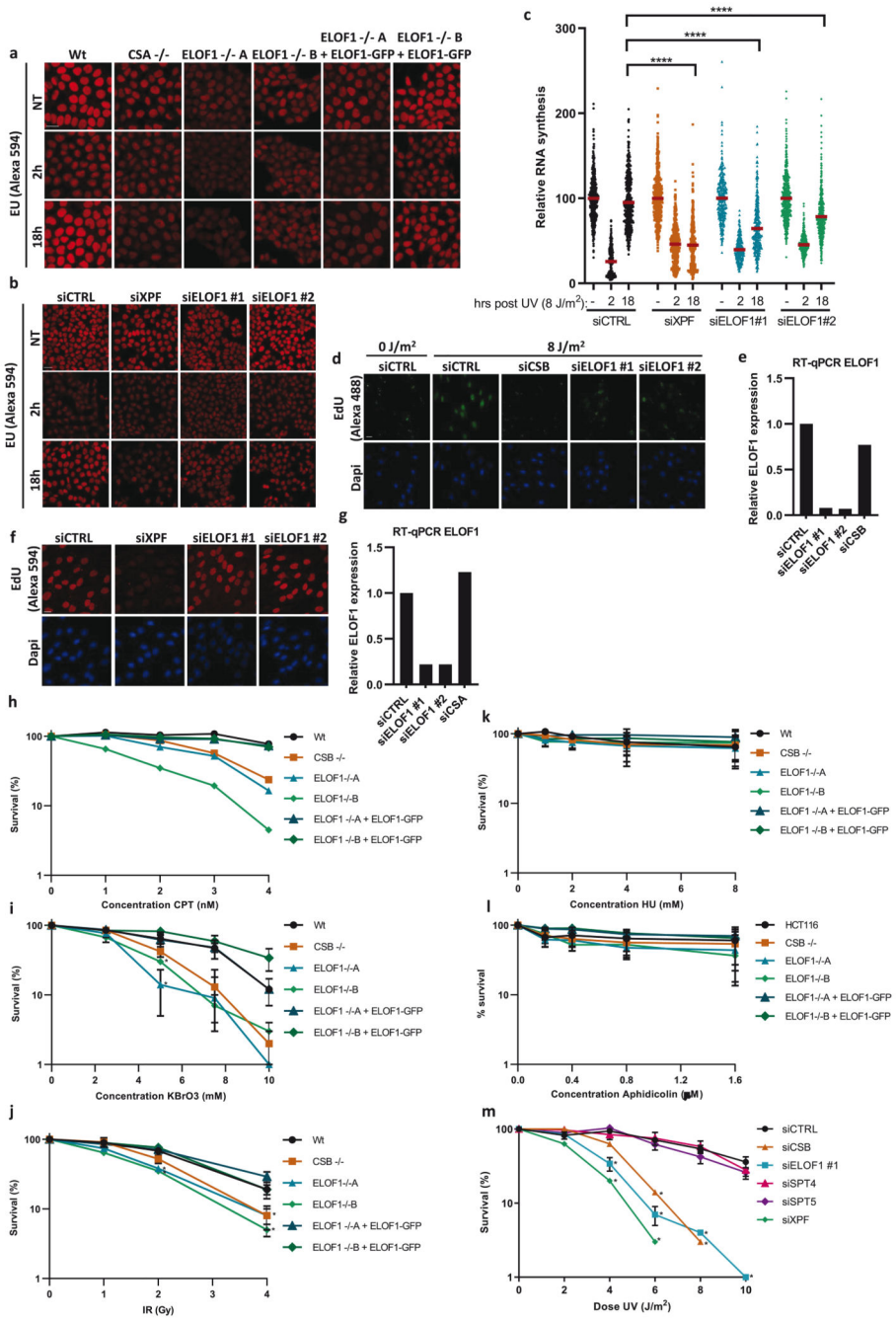

Extended Data Fig. 4. Role of ELOF1 during TC-NER and protection against different DNA damaging agents.

(a+b) Representative immunofluorescence images of EU incorporation in **(a)** indicated HCT116 cells, or **(b)** HCT116 cells transfected with indicated siRNAs, 2 or 18 hours after 8 J/m^2 UV-C or mock treatment (NT). Scale bar: 20 μm. **(c)** Transcription restart after UV damage as determined by relative EU incorporation in HCT116 cells transfected with indicated siRNAs, 2 or 18 hours after 8 J/m^2 UV-C or mock treatment (NT). Relative integrated density of UV-irradiated samples are normalized to mock-treated and set to 100%.

Europe PMC Funders Author Manuscripts

Red lines indicate average integrated density of, respectively n=492, 485, 435, 487, 461, 395, 352, 399, 380, 644, 575, 512 cells collected from three independent experiments. **(d)** Representative immunofluorescence images of amplified EdU signal in XP186LV fibroblasts (XP-C) transfected with indicated siRNAs, 7 hours after exposure to 8 J/m^2 UV-C. Scale bar: 20 μm. TCR-UDS has been performed three times with similar results. **(e)** Relative ELOF1 mRNA levels in XP186LV fibroblasts (XP-C) following transfection with indicated siRNAs determined by RT-qPCR. ELOF1 expression was normalized to GAPDH expression and siCTRL levels were set to 1. Data shown represent average of 2 independent experiments. **(f)** Representative fluorescence images of EdU incorporation 3 hours after irradiation with 16 J/m^2 UV-C in C5RO (hTert) cells transfected with indicated siRNAs. Scale bar: 20 μm. **(g)** as in (f) in C5RO (hTert) cells. Data shown represent average of 2 independent experiments. **(h-k)** Relative colony survival of indicated HCT116 Wt and KO (-/-) cells, with ELOF1 re-expression where indicated, continuously exposed to indicated concentrations of **(h)** camptothecin (CPT) or **(i)** potassium bromate ($KBrO_3$), or irradiated with indicated doses of **(j)** ionizing radiation (IR), or exposed to indicated concentrations of (k) hydroxyurea (HU) or (l) aphidicolin. Plotted curves represent averages ± SEM. CPT: n=2; $KBrO_3$: n=3; IR: n=5; HU: n=3, others n=4 independent experiments. **(m)** Relative colony survival of HCT116 cells transfected with indicated siRNAs following exposure to indicated doses of UV-C. Plotted curves represent averages ± SEM. siCTRL, siSPT4 and siSPT5 n=4, siELOF1 #1, siCSB, siXPF n=2 independent experiments. *P≤0.05, ****p≤0.0001 analyzed by two-sided unpaired T-test in (c) and one-sided unpaired T-test in (h-m). Numerical data are provided in source data extended data fig. 4.

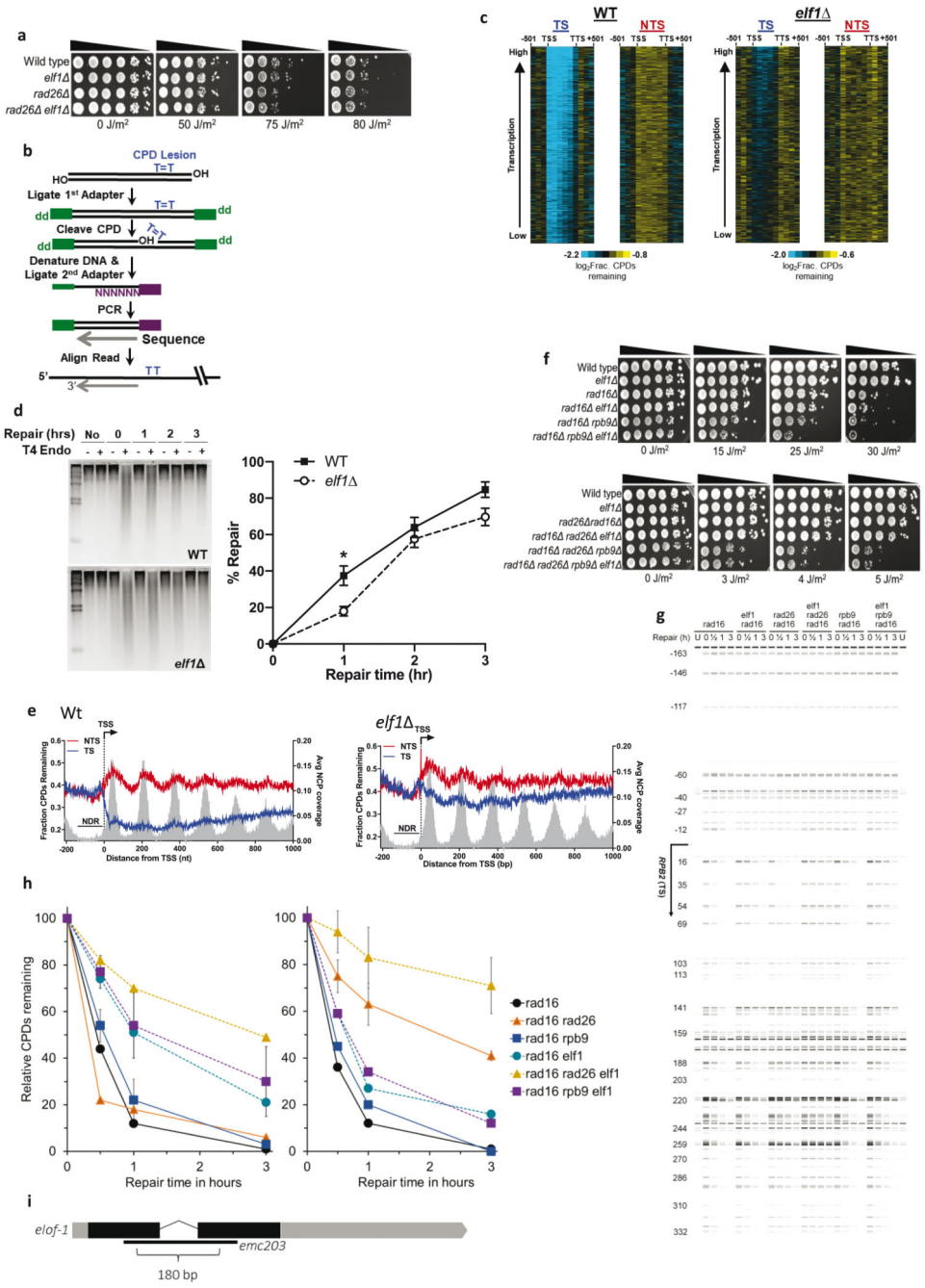

Extended Data Fig. 5. Role of yeast *elf1* in TC-NER.

(a) Indicated mutant yeast strains were serially 10-fold diluted, spotted, and exposed to indicated UV-C doses. Spot assay has been performed three times with similar results. **(b)** Schematic showing the CPD-seq method. Isolated DNA is sonicated and adaptors are ligated. CPDs are cleaved by T4 endonuclease V and APE1 nuclease to generate 3' ends. Following denaturing of the DNA, ends are ligated to a second adaptor that allows CPD sequencing. **(c)** Gene plot analysis of CPD-seq data for ~4500 yeast genes, ordered by transcription frequency[65]. Plots depict unrepaired CPDs following 2-hour repair relative to

Europe PMC Funders Author Manuscripts

no repair for both the transcribed strand (TS) and non-transcribed strand (NTS). Each row represents approximately 10 genes. TSS=transcription start site, TTS=transcription termination site. **(d)** Left panel: Representative gel of bulk repair of UV-induced CPD lesions in Wt and *elf1*Δ mutant yeast measured by T4 endonuclease V digestion and alkaline gel electrophoresis of genomic DNA isolated from UV-irradiated yeast (100 J/m^2 UV-C light) after the indicated time. Right panel: Quantification of CPD repair from n=3 WT and n=4 elf1Δ experiments ±SEM. *$P \leq 0.05$ analyzed by unpaired two-sided t-test. **(e)** Single nucleotide resolution analysis of CPD-seq data downstream of the TSS of ~5200 yeast genes. Plots depict fraction of unrepaired CPDs following 2-hour repair relative to no repair for both TS and NTS. Nucleosome positioning data[50] is shown for reference. **(f)** Controls for UV spotting assays shown in Fig. 4d. **(g)** Image showing repair of CPDs in the TS of the *RPB2* gene for indicated yeast strains. The image was generated by converting sequencing reads aligned to RPB2 into bands. *U:* unirradiated cells. Nucleotide positions relative to TSS (+1) are indicated on the left. **(h)** Left: Relative percentage of CPDs remaining within 54 bp downstream of the TSS of the *RPB2* gene. Right: Relative percentage of CPDs remaining in the downstream region (69-353 bp) of the *RPB2* gene. Data are presented as mean values from all CPD sites within the indicated regions (0-54 and 69-353 bp) of the RPB2 gene ±SD from one single experiment, error bars are shown for most relevant strains. n = 8 sites (left panel), and n = 73 (right panel) is 73. **(i)** Representation of the *C. elegans elof-1* genomic organization, depicting the 180 bp *emc203* deletion allele generated with CRISPR/Cas9. Shaded boxes: exons, black: coding sequences. Numerical data are provided in source data extended data fig. 5.

Europe PMC Funders Author Manuscripts

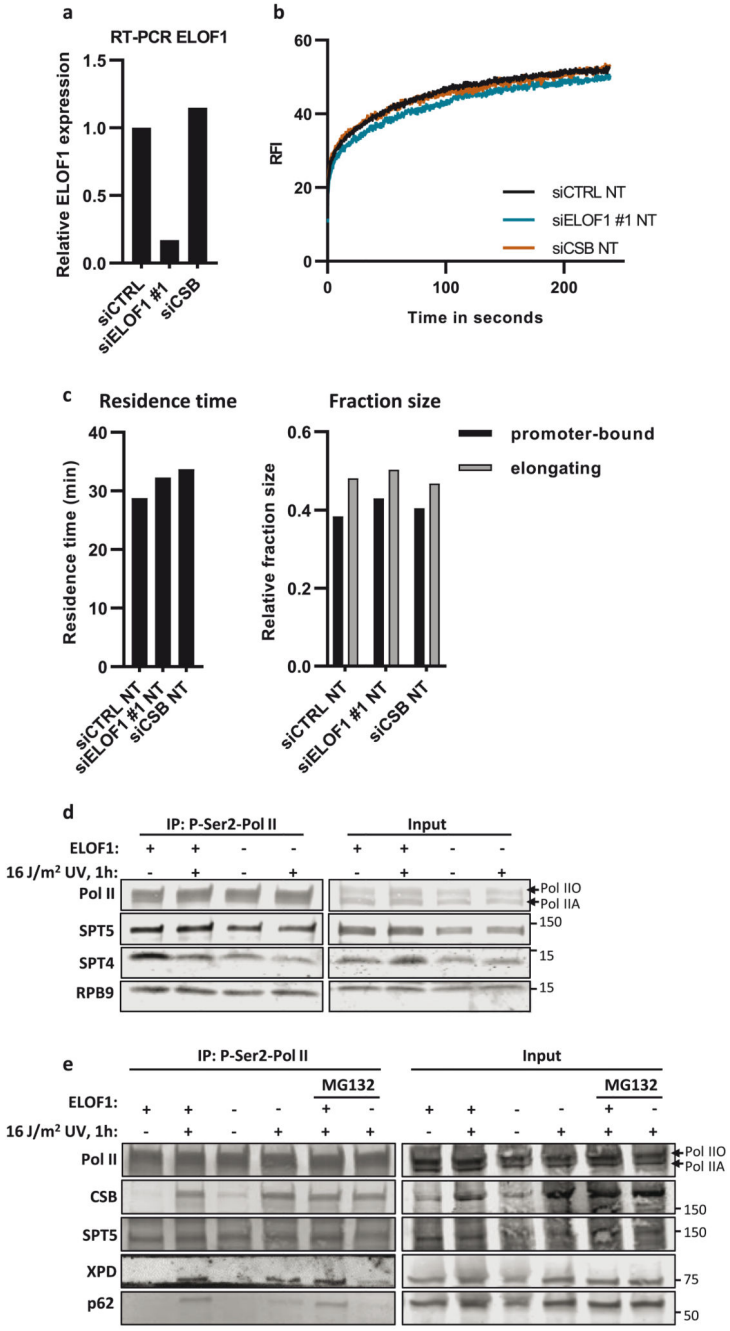

Extended Data Fig. 6. Effects of ELOF1 deficiency on elongating Pol II elongation speed and complex composition.

(a) Relative ELOF1 mRNA levels in *GFP-RPB1* KI cells transfected with indicated siRNAs as determined by RT-qPCR. ELOF1 expression was normalized to GAPDH signal and levels of control cells were set to 1. Data shown represent average of 2 independent experiments. **(b)** FRAP analysis of GFP-RPB1 mobility after depletion of indicated factors. Mock-treated curves corresponding to figure 4A. siCTRL n=28, siELOF1 #1 n=20, siCSB NT n=14 cells analyzed across 4, 3 and 3 independent experiments respectively. **(c)** Left panel: Residence

time of elongating Pol II or right panel: relative fraction size of promoter-bound or elongating Pol II as determined by Monte-Carlo-based modeling of RPB1 mobility as shown in (a). **(d)** Native immunoprecipitation of Pol II in Wt and ELOF -/-A cells followed by immunoblotting for indicated proteins. Cells were harvested 1 hour after mock treatment or irradiation with 16 J/m^2 UV-C. MG132: treatment with 50 μM proteasome inhibitor MG132, 1 hour before UV irradiation. **(e)** Native immunoprecipitation of Pol II in Wt and ELOF -/-A cells followed by immunoblotting for indicated proteins. Cells were harvested 1 hour after mock treatment or irradiation with 16 J/m^2 UV-C. IP experiments depicted in d and e were executed two times with similar results. Numerical data and uncropped blots are provided in source data extended data fig. 6.

Europe PMC Funders Author Manuscripts

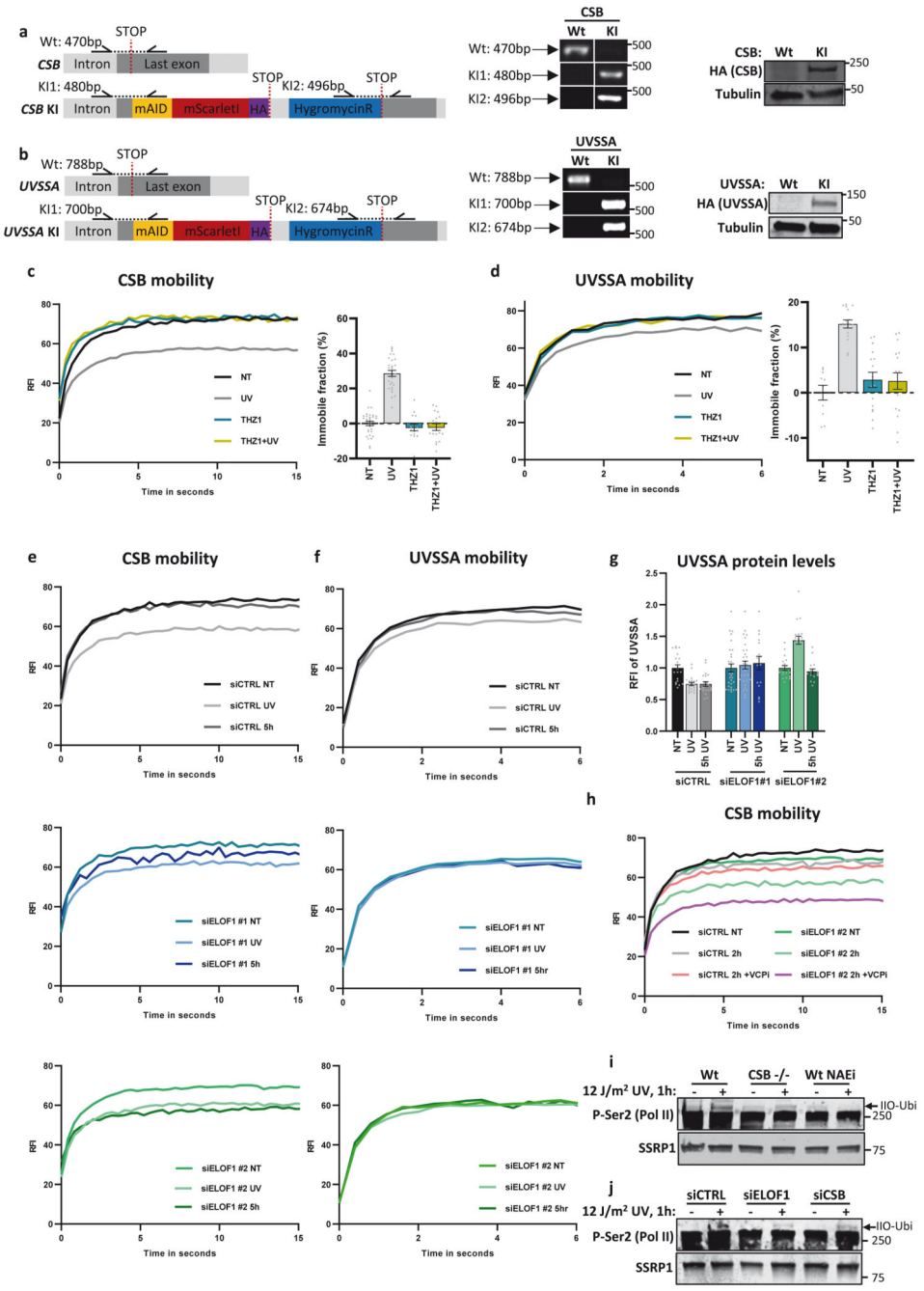

Extended Data Fig. 7. ELOF1 KO impairs recruitment of UVSSA but not CSB.

(a) Left panel: Schematic of the genomic locus of *CSB* and used strategy for generating the homozygous *CSB-mScarletI-HA* KI cell line. Half arrows indicate primer locations. Middle and right panel: Genotyping PCR and immunoblot for *CSB*-KI cell line. **(b)** Left panel: Schematic of the genomic locus of *UVSSA* and used strategy for generating the homozygous *UVSSA- mScarletI-HA* KI cell line. Half arrows indicate primer locations. Middle and right panel: Genotyping PCR and immunoblot for *UVSSA*-KI cell line. Experiments depicted in a and b were performed two times with similar results. **(c)** Left

Europe PMC Funders Author Manuscripts

panel: CSB mobility was determined by FRAP analysis of CSB-mScarletI after the indicated treatments. THZ1: 1 hour treatment (2 μM) before UV-C irradiation (4 J/m^2) or mock treatment. Right panel: Relative immobile fraction of CSB as determined by FRAP analysis. Plotted values represent mean ± SEM and are normalized to mock treated. NT n=32; UV n=28; THZ1 n=15; THZ1+UV n=18 cells analyzed across 2 independent experiments. **(d)** Same as C but for UVSSA-mScarletI. NT n=10; UV n=16; THZ1 n=16; THZ1+UV n=17 cells analyzed across 2 independent experiments. **(e+f)** FRAP analyses of CSB-mScarletI **(e)** or UVSSA-mScarletI **(f)** mobility after transfection with indicated siRNAs in individual graphs. Cells were mock treated (NT) or analyzed directly (UV) or 5 hours (5hr UV) after irradiation with 4 J/m^2 UV-C. **(g)** Relative fluorescence intensity of UVSSA in *UVSSA*-KI cells transfected with indicated siRNAs as determined by live-cell imaging. Plotted values represent mean ± SEM. siCTRL NT n=30, UV+5h UV n=21; siELOF1 #1 NT n=38, UV n=34, 5h UV n=16; siELOF1 #2 NT+UV n=19, 5h UV n=16 cells analyzed across 4 independent experiments for siCTRL and 3 for siELOF1 and siCSB. **(h)** FRAP analysis of CSB in *CSB*-KI cells transfected with indicated siRNAs 2 hours after UV. VCPi: VCP inhibitor (5 μM) was directly added after UV-C (4 J/m^2). **(i)** Immunoblot of chromatin fraction of indicated cell lines 1 hour after 12 J/m^2 UV-C or mock treatment. NAEi = 1 hour treatment with NEDDylation inhibitor (10 μM). SSRP1 is shown as loading control. **(j)** Immunoblot of chromatin fraction of HCT116 cells transfected with indicated siRNAs 1 hour after 12 J/m^2 UV-C or mock treatment. SSRP1 is shown as loading control. Immunoblots depicted in i and j were executed two times with similar results. Numerical data and uncropped blots are provided in source data extended data fig. 7.

Europe PMC Funders Author Manuscripts

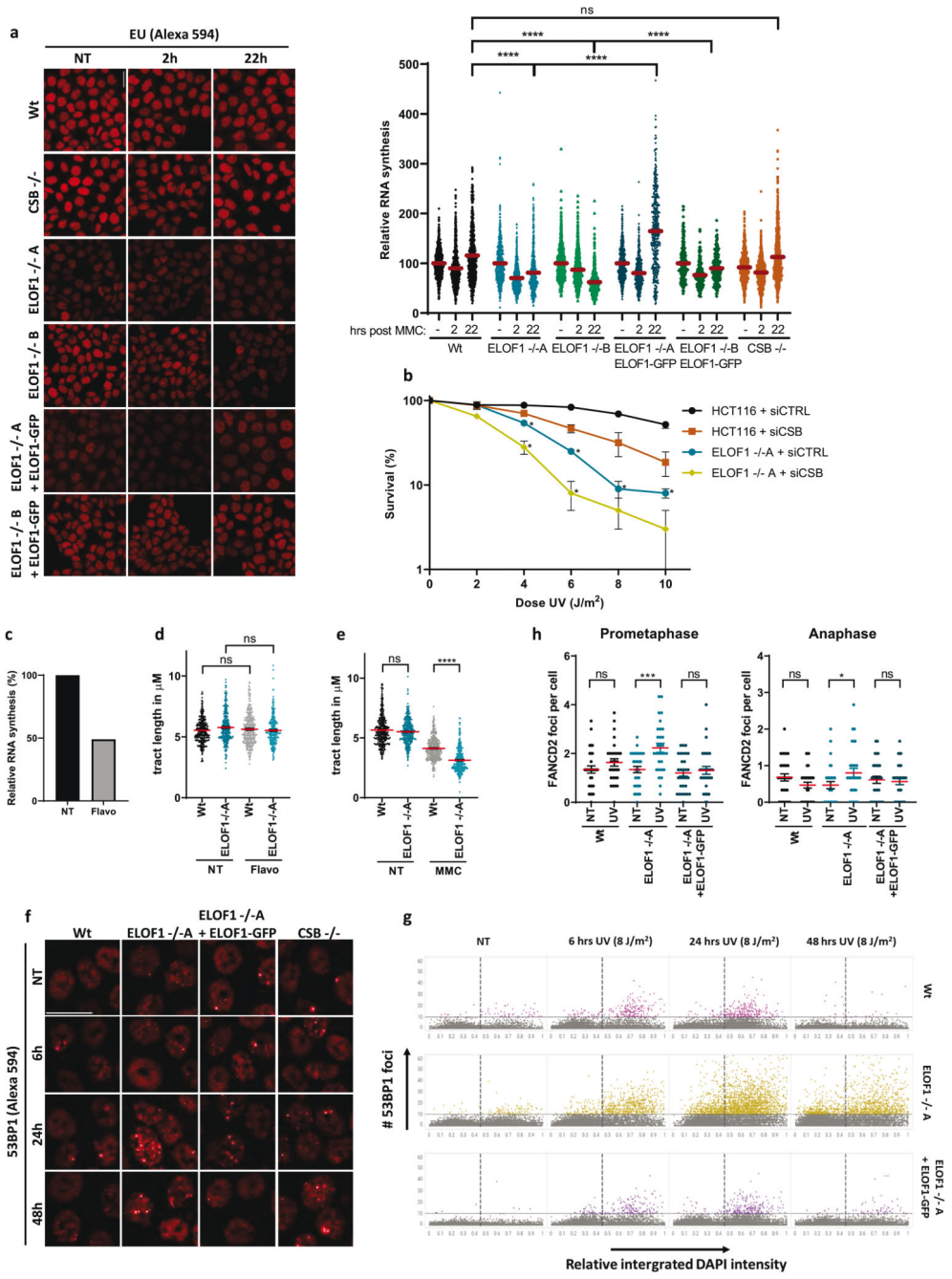

Extended Data Fig. 8. The additional role of ELOF1 in preventing transcription-mediated replication hindrance.

(a) Left panel: Representative immunofluorescence images of EU incorporation in indicated HCT116 cells, untreated, or 2 or 22 hours after a 2-hour exposure to 10 μg/ml mitomycin C. Scale bar: 20 μm. Right panel: Transcription restart after mitomycin C as determined by relative EU incorporation in the indicated HCT116 cells. Mitomycin C-treated samples are normalized to mock treated levels and set to 100%. Red lines indicate average integrated density ± SEM of, respectively, n=1008, 1008 ,727, 938, 960, 715, 1133, 1162, 784, 884, 616, 461, 978, 1013, 693, 221, 220, 206 cells collected from four independent experiments.

(b) Relative colony survival of indicated cell lines with siRNA transfection following exposure to indicated doses of UV-C. Plotted curves represent averages ± SEM, n=3 independent experiments. **(c)** Percentage of RNA synthesis in untreated HCT116 cells and cells treated with 0.1 μM flavopiridol for 2 hours as determined by FACS-based quantification of EU pulse labeling. Experiment has been performed two times with similar results. **(d)** Fork progression measured by tract lengths of CldU (red) in μm is depicted for indicated HCT116 cells, untreated or after 15 minutes 0.1 μM flavopiridol treatment. Tracts of respectively n=300, 300, 304 cells collected from two independent experiments. **(e)** As (d) but after treatment for 1 hour with 25 nM MMC. Tracts of, respectively n=406, 422, 408, 406 cells collected from two independent experiments. **(f)** Representative immunofluorescence images of 53BP1 foci in indicated HCT116 cells, untreated or 6, 24 or 48 hours after exposure to 8 J/m^2 UV-C. Scale bar: 20 μm. **(g)** Number of 53BP1 foci as determined in (f) quantified by Cellprofiler and plotted against normalized integrated intensity of DAPI, respectively, n=10494, 7870, 13916, 16647, 9539, 8313, 8610, 8817, 11253, 10950, 10314, 10494 cells collected from two independent experiments. **(h)** Number of FANCD2 foci per mitosis in prometaphase (left) or anaphase (right) in indicated HCT116 cells in untreated conditions or 48 hours after $4J/m^2$ UV-C. n=90 cells collected from 3 independent experiments for all conditions. *p≤0.05, ***p≤0.001, ****p≤0.0001 analyzed by two-sided unpaired T-test (a), one-sided unpaired T-test (b), Kruskal-Wallis test for multiple comparisons (d,e), and two-sided unpaired t-test (Mann-Whitney) (h). Numerical data are provided in source data extended data fig. 8.

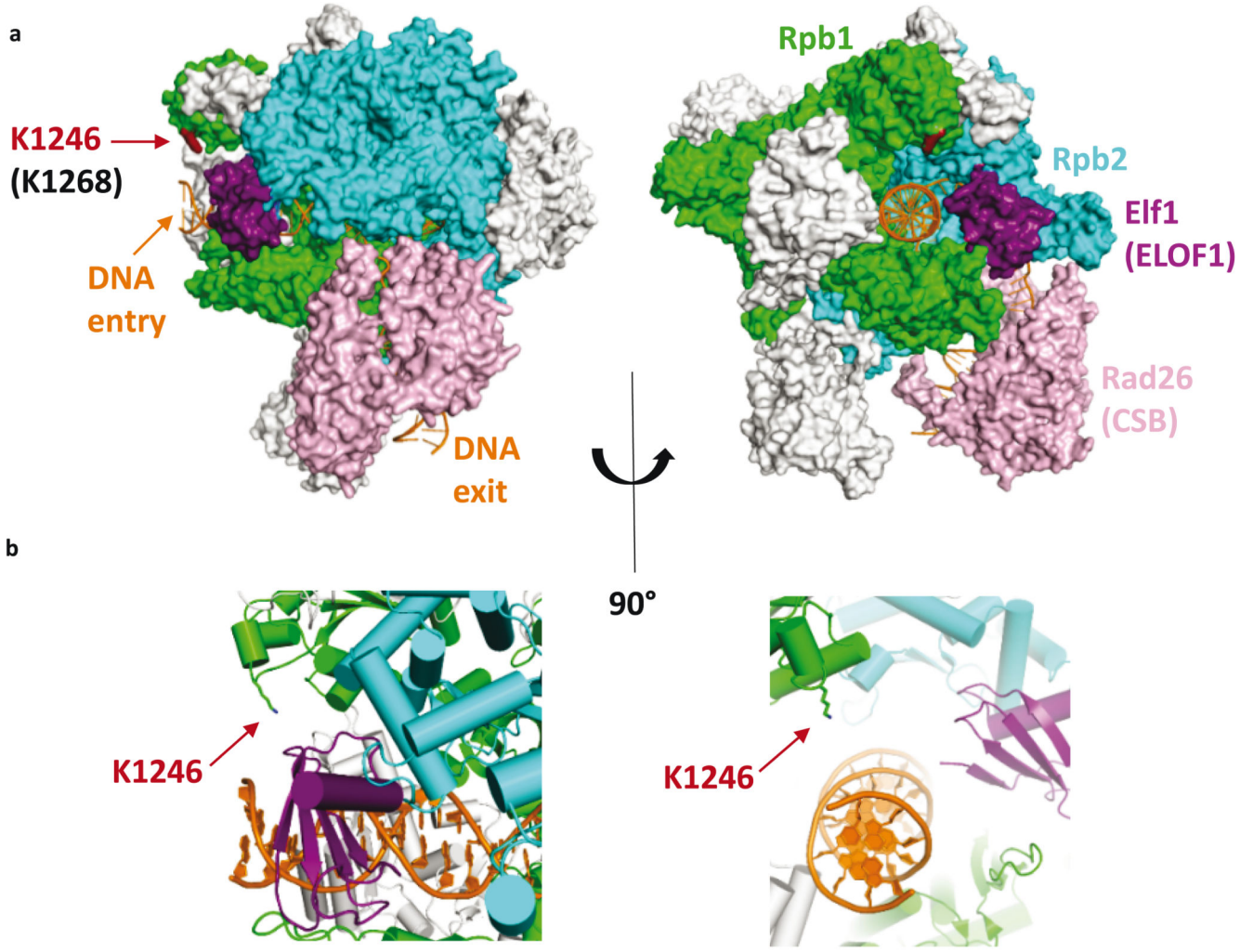

Extended Data Fig. 9. Pol II-ELOF1 complex structure together with CSB.

(a) *S.cerevisiae* Pol II (5vvr.pdb) with Rpb1 in green, Rpb2 in cyan, DNA in orange and Rad26 (CSB) in pink. The *P.pastoris* Pol II in complex with elongation factors (5xog.pdb) was superimposed onto this structure (Rpb1 subunits aligned onto each other), and all subunits except Elf1 (ELOF1; purple) were omitted for clarity. Conserved lysine K1246 (K1268 in mammalian Pol II) is indicated in dark red. **(b)** Close up of Elf1 (ELOF1) binding region.

Supplementary Material

Refer to Web version on PubMed Central for supplementary material.

Acknowledgements

We thank the Optical Imaging Centre and the proteomics center of the Erasmus Medical Center for support with microscopes and mass spectrometry analysis. We thank the Advanced Sequencing Facility of the Francis Crick Institute's for technical assistance on the DRB/TT$_{chem}$-seq. We acknowledge infrastructural support from the Josephine Nefkens Precision Cancer Treatment Program.

Funding

This work is part of the Oncode Institute which is partly financed by the Dutch Cancer Society and was funded by a grant from the Dutch Cancer Society (KWF grant 10506). This work was further funded by the Dutch organization for Scientific Research (NWO-ALW) which awarded a VIDI (864.13.004) and VICI (VI.C.182.025) grant to J.A.M. A.R.C. is supported by the Dutch Cancer Society (KWF grant 11008) and NWO VIDI (193.131). S.L. is funded by the National Science Foundation (MCB-1615550). J.J.W. is funded by the National Institute of Environmental Health Sciences (grants R01ES028698, R21ES029655, and R21ES029302). M.A.T.M.v.V. is funded by a grant from the European Research Council (ERC CoS Grant 682421). H.L. is funded by The Netherlands Organization for Scientific Research (project nr 711.018.007) and Cancergenomics.nl. W.V was funded by a grant from the European Research Council (Agreement 340988). J.Q.S. was supported by the Francis Crick Institute (FCI receives funding from Cancer Research UK [FC001166], the UK Medical Research Council [FC001166], and the Wellcome Trust [FC001166]) and by a grant from the European Research Council (Agreement 693327).

Data availability

All DRB/TT_{chem}-seq data used in this study is available under GEO accession: GSE148844. All CPD-seq data is available under GEO accession: GSE149082. The SILAC-based quantitative interaction proteomics data have been deposited to the ProteomeXchange Consortium via the PRIDE partner repository with the dataset identifier PXD025304. Source data underlying Figs. 1–6 and all Extended data Figures. are provided as a Source Data file with this paper. Any other data are available from the corresponding author upon reasonable request.

References

1. Lans H, Hoeijmakers JHJ, Vermeulen W, Marteijn JA. The DNA damage response to transcription stress. Nat Rev Mol Cell Biol. 2019; 20:766–784. [PubMed: 31558824]
2. Gomez-Gonzalez B, Aguilera A. Transcription-mediated replication hindrance: a major driver of genome instability. Genes Dev. 2019; 33:1008–1026. [PubMed: 31123061]
3. Gaillard H, Aguilera A. Transcription as a Threat to Genome Integrity. Annu Rev Biochem. 2016; 85:291–317. [PubMed: 27023844]
4. Laugel V. Cockayne syndrome: the expanding clinical and mutational spectrum. Mech Ageing Dev. 2013; 134:161–170. [PubMed: 23428416]
5. Xu J, et al. Structural basis for the initiation of eukaryotic transcription-coupled DNA repair. Nature. 2017; 551:653–657. [PubMed: 29168508]
6. Groisman R, et al. CSA-dependent degradation of CSB by the ubiquitin-proteasome pathway establishes a link between complementation factors of the Cockayne syndrome. Genes Dev. 2006; 20:1429–1434. [PubMed: 16751180]
7. van der Weegen Y, et al. The cooperative action of CSB, CSA, and UVSSA target TFIIH to DNA damage-stalled RNA polymerase II. Nat Commun. 2020; 11:2104. [PubMed: 32355176]
8. Nakazawa Y, et al. Ubiquitination of DNA Damage-Stalled RNAPII Promotes Transcription-Coupled Repair. Cell. 2020; 180:1228–1244. e1224 [PubMed: 32142649]
9. Tufegdzic Vidakovic A, et al. Regulation of the RNAPII Pool Is Integral to the DNA Damage Response. Cell. 2020; 180:1245–1261. e1221 [PubMed: 32142654]
10. Okuda M, Nakazawa Y, Guo C, Ogi T, Nishimura Y. Common TFIIH recruitment mechanism in global genome and transcription-coupled repair subpathways. Nucleic acids research. 2017; 45:13043–13055. [PubMed: 29069470]
11. Scharer OD. Nucleotide excision repair in eukaryotes. Cold Spring Harb Perspect Biol. 2013; 5 a012609 [PubMed: 24086042]
12. Sanjana NE, Shalem O, Zhang F. Improved vectors and genome-wide libraries for CRISPR screening. Nat Methods. 2014; 11:783–784. [PubMed: 25075903]
13. Li W, et al. MAGeCK enables robust identification of essential genes from genome-scale CRISPR/Cas9 knockout screens. Genome Biol. 2014; 15:554. [PubMed: 25476604]

14. Yang W, Gao Y. Translesion and Repair DNA Polymerases: Diverse Structure and Mechanism. Annu Rev Biochem. 2018; 87:239–261. [PubMed: 29494238]
15. Daniels JP, Kelly S, Wickstead B, Gull K. Identification of a crenarchaeal orthologue of Elf1: implications for chromatin and transcription in Archaea. Biol Direct. 2009; 4:24. [PubMed: 19640276]
16. Prather D, Krogan NJ, Emili A, Greenblatt JF, Winston F. Identification and characterization of Elf1, a conserved transcription elongation factor in Saccharomyces cerevisiae. Mol Cell Biol. 2005; 25:10122–10135. [PubMed: 16260625]
17. Joo YJ, Ficarro SB, Chun Y, Marto JA, Buratowski S. In vitro analysis of RNA polymerase II elongation complex dynamics. Genes Dev. 2019; 33:578–589. [PubMed: 30846429]
18. Ehara H, et al. Structure of the complete elongation complex of RNA polymerase II with basal factors. Science. 2017; 357:921–924. [PubMed: 28775211]
19. Mayer A, et al. Uniform transitions of the general RNA polymerase II transcription complex. Nat Struct Mol Biol. 2010; 17:1272–1278. [PubMed: 20818391]
20. Ehara H, et al. Structural insight into nucleosome transcription by RNA polymerase II with elongation factors. Science. 2019; 363:744–747. [PubMed: 30733384]
21. Steurer B, et al. Fluorescently-labelled CPD and 6-4PP photolyases: new tools for live-cell DNA damage quantification and laser-assisted repair. Nucleic acids research. 2019; 47:3536–3549. [PubMed: 30698791]
22. Steurer B, et al. Live-cell analysis of endogenous GFP-RPB1 uncovers rapid turnover of initiating and promoter-paused RNA Polymerase II. Proc Natl Acad Sci U S A. 2018; 115:E4368–E4376. [PubMed: 29632207]
23. van den Boom V, et al. DNA damage stabilizes interaction of CSB with the transcription elongation machinery. J Cell Biol. 2004; 166:27–36. [PubMed: 15226310]
24. Gregersen LH, Mitter R, Svejstrup JQ. Using TTchem-seq for profiling nascent transcription and measuring transcript elongation. Nat Protoc. 2020; 15:604–627. [PubMed: 31915390]
25. Nudler E. RNA polymerase backtracking in gene regulation and genome instability. Cell. 2012; 149:1438–1445. [PubMed: 22726433]
26. Jia N, et al. A rapid, comprehensive system for assaying DNA repair activity and cytotoxic effects of DNA-damaging reagents. Nat Protoc. 2015; 10:12–24. [PubMed: 25474029]
27. Wienholz F, Vermeulen W, Marteijn JA. Amplification of unscheduled DNA synthesis signal enables fluorescence-based single cell quantification of transcription-coupled nucleotide excision repair. Nucleic acids research. 2017; 45:e68. [PubMed: 28088761]
28. Jaspers NG, et al. Anti-tumour compounds illudin S and Irofulven induce DNA lesions ignored by global repair and exclusively processed by transcription- and replication-coupled repair pathways. DNA Repair (Amst). 2002; 1:1027–1038. [PubMed: 12531012]
29. Slyskova J, et al. Base and nucleotide excision repair facilitate resolution of platinum drugs-induced transcription blockage. Nucleic acids research. 2018; 46:9537–9549. [PubMed: 30137419]
30. Veloso A, et al. Genome-wide transcriptional effects of the anti-cancer agent camptothecin. PLoS One. 2013; 8 e78190 [PubMed: 24194914]
31. Brooks PJ, et al. The oxidative DNA lesion 8,5'-(S)-cyclo-2'-deoxyadenosine is repaired by the nucleotide excision repair pathway and blocks gene expression in mammalian cells. J Biol Chem. 2000; 275:22355–22362. [PubMed: 10801836]
32. van Gool AJ, et al. RAD26, the functional S. cerevisiae homolog of the Cockayne syndrome B gene ERCC6. EMBO J. 1994; 13:5361–5369. [PubMed: 7957102]
33. Mao P, Smerdon MJ, Roberts SA, Wyrick JJ. Chromosomal landscape of UV damage formation and repair at single-nucleotide resolution. Proc Natl Acad Sci U S A. 2016; 113:9057–9062. [PubMed: 27457959]
34. Duan M, Selvam K, Wyrick JJ, Mao P. Genome-wide role of Rad26 in promoting transcription-coupled nucleotide excision repair in yeast chromatin. Proc Natl Acad Sci U S A. 2020; 117:18608–18616. [PubMed: 32690696]
35. Li S, Smerdon MJ. Rpb4 and Rpb9 mediate subpathways of transcription-coupled DNA repair in Saccharomyces cerevisiae. EMBO J. 2002; 21:5921–5929. [PubMed: 12411509]

36. Lans H, et al. Involvement of global genome repair, transcription coupled repair, and chromatin remodeling in UV DNA damage response changes during development. PLoS Genet. 2010; 6 e1000941 [PubMed: 20463888]
37. Williamson L, et al. UV Irradiation Induces a Non-coding RNA that Functionally Opposes the Protein Encoded by the Same Gene. Cell. 2017; 168:843–855. e813 [PubMed: 28215706]
38. Schwertman P, et al. UV-sensitive syndrome protein UVSSA recruits USP7 to regulate transcription-coupled repair. Nature genetics. 2012; 44:598–602. [PubMed: 22466611]
39. He J, Zhu Q, Wani G, Sharma N, Wani AA. Valosin-containing Protein (VCP)/p97 Segregase Mediates Proteolytic Processing of Cockayne Syndrome Group B (CSB) in Damaged Chromatin. J Biol Chem. 2016; 291:7396–7408. [PubMed: 26826127]
40. Lukas C, et al. 53BP1 nuclear bodies form around DNA lesions generated by mitotic transmission of chromosomes under replication stress. Nat Cell Biol. 2011; 13:243–253. [PubMed: 21317883]
41. Minocherhomji S, et al. Replication stress activates DNA repair synthesis in mitosis. Nature. 2015; 528:286–290. [PubMed: 26633632]
42. Schoonen PM, et al. Progression through mitosis promotes PARP inhibitor-induced cytotoxicity in homologous recombination-deficient cancer cells. Nat Commun. 2017; 8 15981 [PubMed: 28714471]
43. Olivieri M, et al. A Genetic Map of the Response to DNA Damage in Human Cells. Cell. 2020; 182:481–496. e421 [PubMed: 32649862]
44. Tellier AP, Archambault D, Tremblay KD, Mager J. The elongation factor Elof1 is required for mammalian gastrulation. PLoS One. 2019; 14 e0219410 [PubMed: 31276560]
45. Wienholz F, et al. FACT subunit Spt16 controls UVSSA recruitment to lesion-stalled RNA Pol II and stimulates TC-NER. Nucleic acids research. 2019
46. Fei J, Chen J. KIAA1530 protein is recruited by Cockayne syndrome complementation group protein A (CSA) to participate in transcription-coupled repair (TCR). J Biol Chem. 2012; 287:35118–35126. [PubMed: 22902626]
47. Evers B, et al. CRISPR knockout screening outperforms shRNA and CRISPRi in identifying essential genes. Nat Biotechnol. 2016; 34:631–633. [PubMed: 27111720]
48. Nilson KA, et al. THZ1 Reveals Roles for Cdk7 in Co-transcriptional Capping and Pausing. Mol Cell. 2015; 59:576–587. [PubMed: 26257281]
49. Chao SH, et al. Flavopiridol inhibits P-TEFb and blocks HIV-1 replication. J Biol Chem. 2000; 275:28345–28348. [PubMed: 10906320]
50. Weiner A, et al. High-Resolution Chromatin Dynamics during a Yeast Stress Response. Molecular Cell. 2015; 58:371–386. [PubMed: 25801168]
51. Campeau E, et al. A Versatile Viral System for Expression and Depletion of Proteins in Mammalian Cells. PLOS ONE. 2009; 4 e6529 [PubMed: 19657394]
52. Yesbolatova A, Natsume T, Hayashi K-i, Kanemaki MT. Generation of conditional auxin-inducible degron (AID) cells and tight control of degron-fused proteins using the degradation inhibitor auxinole. Methods. 2019; 164-165:73–80. [PubMed: 31026591]
53. Natsume T, Kiyomitsu T, Saga Y, Kanemaki MT. Rapid Protein Depletion in Human Cells by Auxin-Inducible Degron Tagging with Short Homology Donors. Cell Rep. 2016; 15:210–218. [PubMed: 27052166]
54. Brinkman EK, Chen T, Amendola M, van Steensel B. Easy quantitative assessment of genome editing by sequence trace decomposition. Nucleic acids research. 2014; 42 e168-e168 [PubMed: 25300484]
55. Shalem O, et al. Genome-Scale CRISPR-Cas9 Knockout Screening in Human Cells. Science. 2014; 343:84–87. [PubMed: 24336571]
56. Livak KJ, Schmittgen TD. Analysis of Relative Gene Expression Data Using Real-Time Quantitative PCR and the 2−ΔΔCT Method. Methods. 2001; 25:402–408. [PubMed: 11846609]
57. Ramirez F, et al. deepTools2: a next generation web server for deep-sequencing data analysis. Nucleic acids research. 2016; 44:W160–165. [PubMed: 27079975]
58. Gardner JM, Jaspersen SL. Manipulating the yeast genome: deletion, mutation, and tagging by PCR. Methods Mol Biol. 2014; 1205:45–78. [PubMed: 25213239]

59. Brachmann CB, et al. Designer deletion strains derived from Saccharomyces cerevisiae S288C: a useful set of strains and plasmids for PCR-mediated gene disruption and other applications. Yeast. 1998; 14:115–132. [PubMed: 9483801]
60. Langmead B, Salzberg SL. Fast gapped-read alignment with Bowtie 2. Nat Methods. 2012; 9:357–359. [PubMed: 22388286]
61. Mao P, Smerdon MJ, Roberts SA, Wyrick JJ. Asymmetric repair of UV damage in nucleosomes imposes a DNA strand polarity on somatic mutations in skin cancer. Genome Res. 2020; 30:12–21. [PubMed: 31871068]
62. Park D, Morris AR, Battenhouse A, Iyer VR. Simultaneous mapping of transcript ends at single-nucleotide resolution and identification of widespread promoter-associated non-coding RNA governed by TATA elements. Nucleic acids research. 2014; 42:3736–3749. [PubMed: 24413663]
63. Eisen MB, Spellman PT, Brown PO, Botstein D. Cluster analysis and display of genome-wide expression patterns. Proceedings of the National Academy of Sciences. 1998; 95:14863.
64. Saldanha AJ. Java Treeview--extensible visualization of microarray data. Bioinformatics. 2004; 20:3246–3248. [PubMed: 15180930]
65. Holstege FC, et al. Dissecting the regulatory circuitry of a eukaryotic genome. Cell. 1998; 95:717–728. [PubMed: 9845373]
66. Mao P, et al. Genome-wide maps of alkylation damage, repair, and mutagenesis in yeast reveal mechanisms of mutational heterogeneity. Genome Res. 2017; 27:1674–1684. [PubMed: 28912372]
67. Hodges AJ, Plummer DA, Wyrick JJ. NuA4 acetyltransferase is required for efficient nucleotide excision repair in yeast. DNA Repair (Amst). 2019; 73:91–98. [PubMed: 30473425]
68. Li M, Ko T, Li S. High-resolution Digital Mapping of N-Methylpurines in Human Cells Reveals Modulation of Their Induction and Repair by Nearest-neighbor Nucleotides. J Biol Chem. 2015; 290:23148–23161. [PubMed: 26240148]
69. Mukherjee C, et al. RIF1 promotes replication fork protection and efficient restart to maintain genome stability. Nature Communications. 2019; 10 3287
70. Callen E, et al. ATM prevents the persistence and propagation of chromosome breaks in lymphocytes. Cell. 2007; 130:63–75. [PubMed: 17599403]
71. Cornacchia D, et al. Mouse Rif1 is a key regulator of the replication-timing programme in mammalian cells. Embo J. 2012; 31:3678–3690. [PubMed: 22850673]
72. van Cuijk L, et al. SUMO and ubiquitin-dependent XPC exchange drives nucleotide excision repair. Nat Commun. 2015; 6 7499 [PubMed: 26151477]

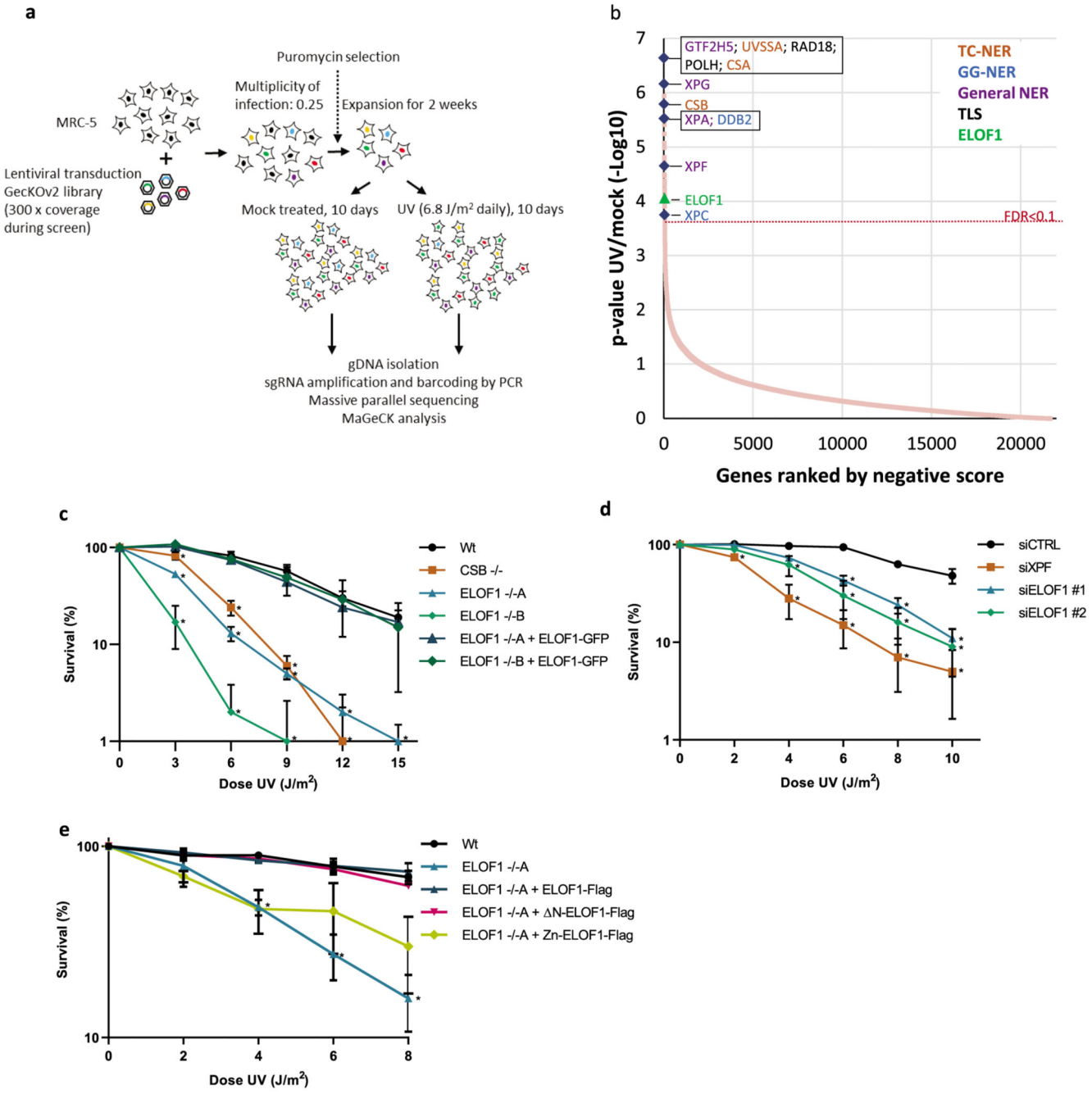

Figure 1. Genome-wide CRISPR/cas9 screen identifies ELOF1 as a factor involved in the UV-induced DNA damage response.

(a) Schematic of the CRISPR/cas9 screen. MRC-5 (SV40) cells were transduced with a lentiviral sgRNA library[12]. The resulting pool of gene-edited cells was split into a control and a UV irradiated group. Cells were respectively mock-treated or daily UV-irradiated with 6.8 J/m^2 UV-C for 10 consecutive days, thereby maintaining ~50% cell confluency throughout the screen (Extended data Fig.1a). sgRNA abundance was determined by next-generation sequencing of PCR-amplified incorporated sgRNAs from the isolated genomic

Europe PMC Funders Author Manuscripts

Europe PMC Funders Author Manuscripts

DNA of surviving cell pools[47]. UV-sensitive genes were identified by comparing the abundance in UV-irradiated cells over mock-treated cells using MAGeCK analysis. The screen was performed in duplicate. **(b)** UV-sensitive genes were ranked based on the gene-based P-value resulting from MaGecK analysis of the change in abundance of sgRNAs in UV-treated over mock-treated. Dotted line indicates FDR=0.1. Genes involved in NER or TLS are color-coded. **(c)** Relative colony survival of HCT116 wildtype (Wt) cells, indicated knock-out cells (-/-) or rescued cells exposed to the indicated doses of UV-C. **(d)** Relative colony survival of MRC-5 cells transfected with indicated siRNAs following exposure to the indicated doses of UV-C. **(e)** Relative colony survival of HCT116 ELOF1 KO cells with expression of the indicated ELOF1 mutants following exposure to the indicated doses of UV-C. Zn: zinc-finger mutant, ΔN: deletion of N-terminus. Data shown in c-e represent average ± SEM (n = 3 independent experiments) *P≤0.05 relative to Wt/siCTRL analyzed by one-sided unpaired T-test. Numerical data are provided in source data fig. 1.

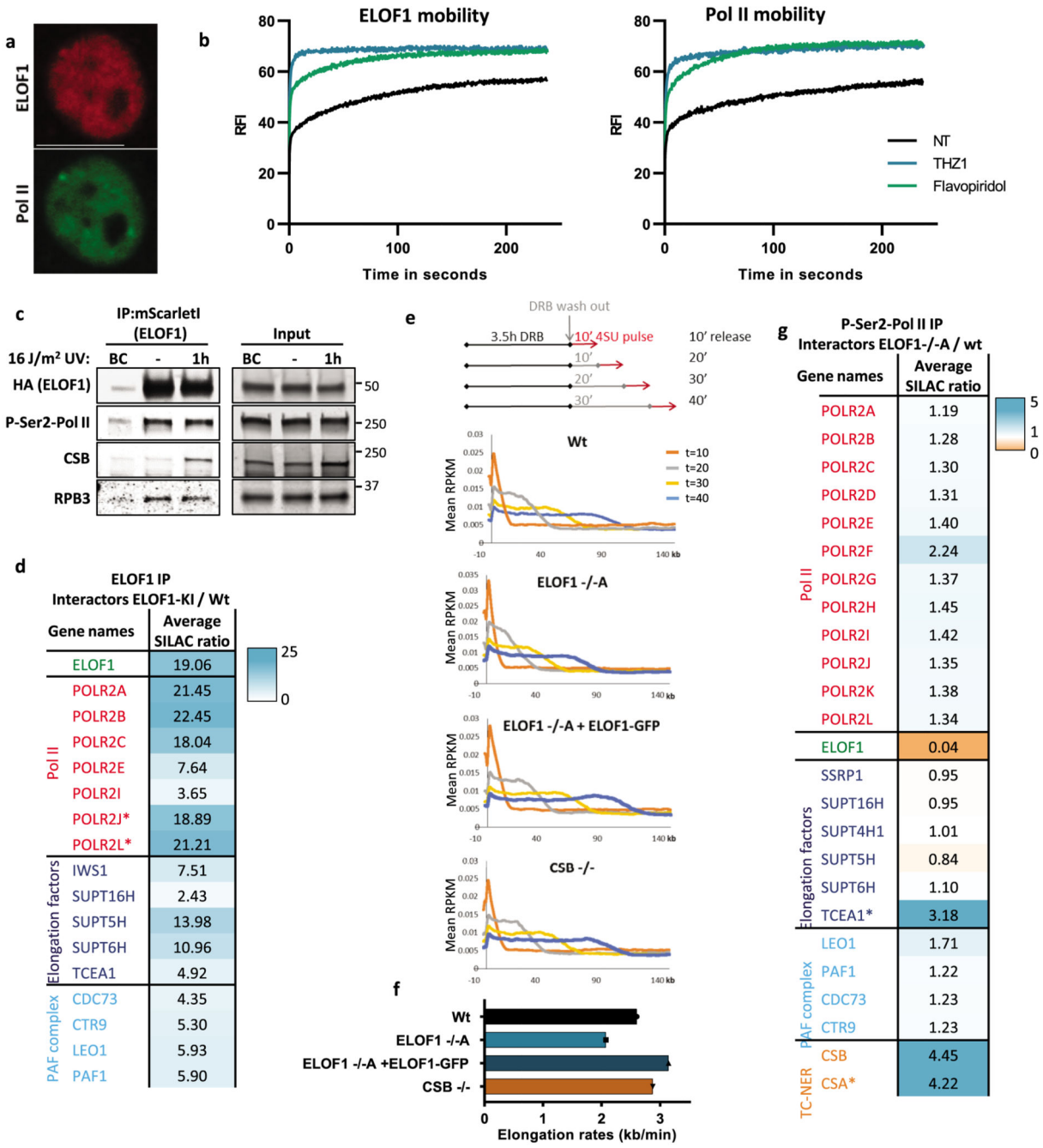

Figure 2. ELOF1 is part of the elongating Pol II complex.

(a) Co-localization of endogenously expressed ELOF1 and Pol II in HCT116 cells with ELOF1-mScarletI-HA and GFP-RPB1 knock-in cells during live-cell imaging. Scale bar: 10 μm. Experiment has been performed 2 times with similar results. **(b)** Fluorescence recovery after photobleaching (FRAP) analysis of endogenously expressed ELOF1-mScarletI (Left) and GFP-RPB1 (Right). Cells were mock-treated (NT) or inhibited at different steps of the transcription cycle using indicated inhibitors. Pol II initiation was inhibited with the CDK7 inhibitor THZ1[48], or promoter-pause release was inhibited by the CDK9 inhibitor

Flavopiridol[49]. Relative Fluorescence Intensity (RFI) was measured over time, background-corrected, and normalized to pre-bleach fluorescence intensity. *ELOF1*-KI: NT n=40, THZ1 n=24, Flavopiridol n=24 and *RPB1*-KI: NT n=21, THZ1 n=16, Flavopiridol n=18 cells across 3 independent experiments. **(c)** Immunoprecipitation of ELOF1 using RFP beads in *ELOF1*-KI cells followed by immunoblotting for indicated proteins. Cells were harvested 1 hour after mock treatment or irradiation with 16 J/m^2 UV-C. BC: binding control. Experiment has been performed 2 times with similar results. **(d)** Interaction heat map of the SILAC ratios of ELOF1-interacting proteins as determined by quantitative interaction proteomics following HA-IP of ELOF1. Average SILAC ratios of duplicate experiments are plotted and represent ELOF1-interactors relative to empty beads. SILAC ratio >1 indicate increase in interaction. * indicates proteins quantified in one experiment. **(e)** Top panel: Schematic of DRB/TT_{chem}-seq to measure Pol II elongation rates. Bottom panel: Metagene profiles of >200 kb genes, of DRB/TT_{chem}-seq in HCT116 Wt or indicated KO (-/-) cells, with ELOF1 re-expression where indicated, 10, 20, 30, or 40 minutes after DRB release. **(f)** Average elongation rates as determined by DRB/TT_{chem}-seq for >200 kb genes. **(g)** Interaction heat map based on the SILAC ratios as determined by quantitative interaction proteomics of P-Ser2-modified Pol II-interacting proteins in ELOF1 -/-A cells relative to Wt cells. Average SILAC ratios of duplicate experiments are plotted. * indicates proteins quantified in one experiment. SILAC ratios <1 indicate loss of interaction, >1 indicate increase in interaction. Numerical data and uncropped blots are provided in source data fig. 2.

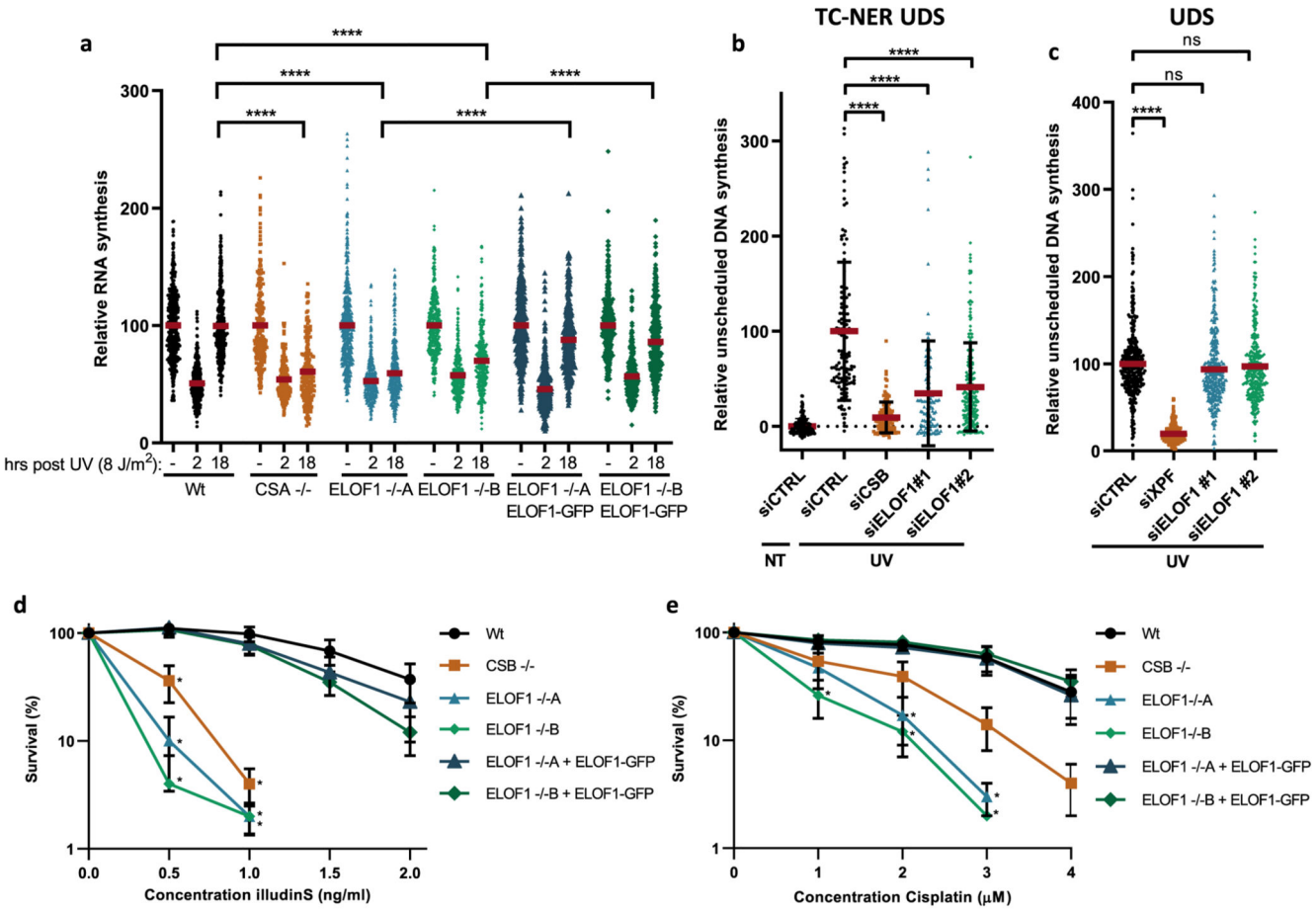

Figure 3. ELOF1 is important for functional TC-NER.

(a) Transcription restart after UV damage as determined by relative EU incorporation in the indicated HCT116 Wt and KO (-/-) cells, with ELOF1 re-expression where indicated, at the indicated time points after UV-C (8 J/m^2). Relative integrated density normalized to mock-treated levels and set to 100%. Red lines indicate average integrated density ± SEM from three independent experiments of respectively, n=537, 528, 496, 227, 222, 203, 455, 421, 431, 458, 450, 405, 499, 495, 406, 470, 432, 446 cells. **(b)** TC-NER-specific UDS as determined by relative EdU incorporation in XP186LV fibroblasts (XP-C) transfected with indicated siRNAs following UV-C-irradiation (7 hours, 8 J/m^2). Cells from two independent experiments. NT: siCTRL n=193; UV: siCTRL n=127, siCSB n=132, siELOF1 #1 n=108, siELOF1 #2 n=217. **(c)** Relative levels of EdU incorporation in C5RO (hTert) cells transfected with indicated siRNAs, following UV-C-irradiation (3 hours, 16 J/m^2). Cells from three independent experiments. siCTRL n=356, siXPF n=203, siELOF1 #1 n=363, siELOF1 #2 n=348. **(d+e)** Relative colony survival of the indicated HCT116 Wt and KO (-/-) cells, with ELOF1 re-expression where indicated, upon a 24-hour exposure to the indicated concentrations of illudinS **(d)** or Cisplatin **(e).** IlludinS: average ± SEM (n=3 independent experiments) for all conditions except ELOF1 -/-B: n=2 independent experiments; Cisplatin: n=4 independent experiments. *p≤0.05, ****p≤0.0001, ns non-

Europe PMC Funders Author Manuscripts

significant, two-sided unpaired T-test in (a,b,c), and one-sided unpaired T-test in (d,e). Numerical data are provided in source data fig. 3.

Europe PMC Funders Author Manuscripts

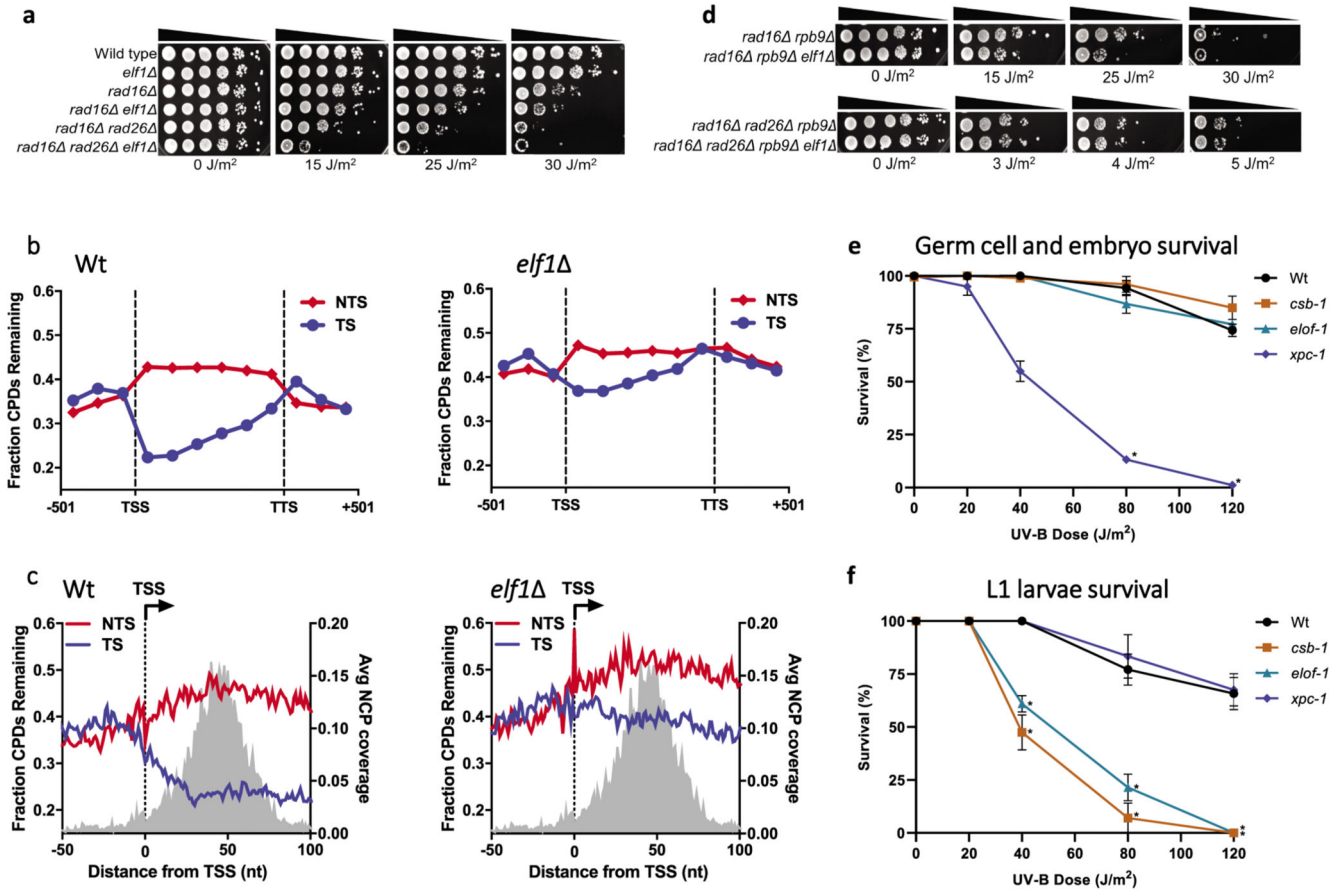

Figure 4. ELOF1 is an evolutionary-conserved TC-NER factor

(a) Indicated mutant yeast strains were serially 10-fold diluted, spotted, and exposed to the indicated UV-C doses. Spot assay has been performed three times with similar results. **(b)** CPD-seq analysis of Wt (left) and *elf1Δ* mutant (right) yeast showing the average fraction of unrepaired CPDs remaining on the transcribed strand (TS) and non-transcribed strand (NTS) for ~5000 yeast genes following 2-hour repair relative to no repair. Each gene was divided in 6 equally-sized bins. Repair in flanking DNA upstream of the transcription start site (TSS) and downstream of the transcription termination site (TTS) is also depicted. **(c)** Close-up of CPD-seq repair data near the TSS in Wt (left) and *elf1Δ* mutant (right) cells. Nucleosome positioning data[50] is shown for reference. CPD-seq has been executed once. **(d)** Indicated mutant yeast strains were serially 10-fold diluted, spotted, and exposed to the indicated UV-C doses. Spot assay has been performed three times with similar results. **(e)** *C. elegans* germ cell and embryo UV survival assay, measuring GG-NER activity, of wild type, *csb-1, xpc-1,* and *elof-1* animals. The percentages of hatched eggs (survival) are plotted against the applied UV-B doses. **(f)** L1 larvae UV survival assay, measuring TC-NER activity, of wildtype, *csb-1*, *xpc-1* and *elof-1* animals. The percentages of animals that developed beyond the L2 stage (survival) are plotted against the applied UV-B doses. In e and f, the mean survival ± SEM of n = three independent experiments each performed in quintuple is depicted. *p≤0.05, ****p≤0.0001. Numerical data are provided in source data fig. 4.

Europe PMC Funders Author Manuscripts

Europe PMC Funders Author Manuscripts

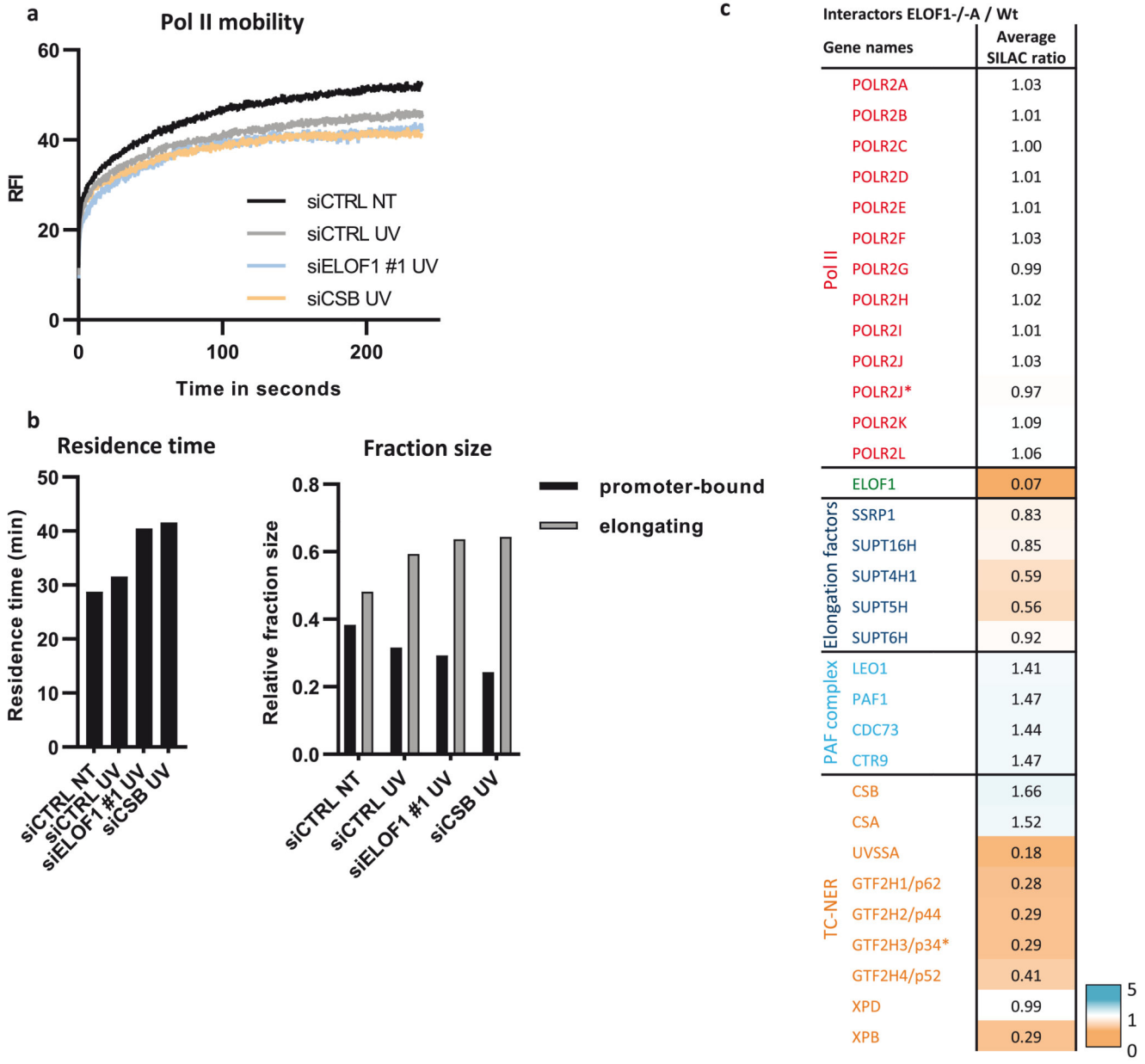

Figure 5. Prolonged stalling of Pol II at TBLs in absence of ELOF1.

(a) FRAP analysis of Pol II mobility in MRC-5 *GFP-RPB1* KI cells after depletion of indicated factors in untreated cells (NT) or directly after UV induction (UV, 12 J/m^2). Relative Fluorescence Intensity (RFI) was measured over time, background-corrected, and normalized to pre-bleach fluorescence intensity. siCTRL NT: n=28, siCTRL UV. n=30, siELOF1 #1 UV n=17, siCSB UV n=24 cells analyzed across four independent experiments for siCTRL and three for siELOF1 and siCSB. **(b)** Left panel: residence time of the elongating Pol II fraction. Right panel: relative fraction sizes of promoter-bound or elongating Pol II as determined by Monte-Carlo-based modeling based on the RPB1 mobility shown in (a). **(c)** Interaction heat map based on the SILAC ratios as determined by

quantitative interaction proteomics of UV-specific Pol II-interacting proteins in ELOF1 -/-A cells relative to Wt cells. Average SILAC ratios of duplicate experiments are plotted. SILAC ratios <1 indicate loss of interaction, >1 indicate increase in interaction. * indicates proteins quantified in one experiment. Numerical data are provided in source data fig. 5.

Europe PMC Funders Author Manuscripts

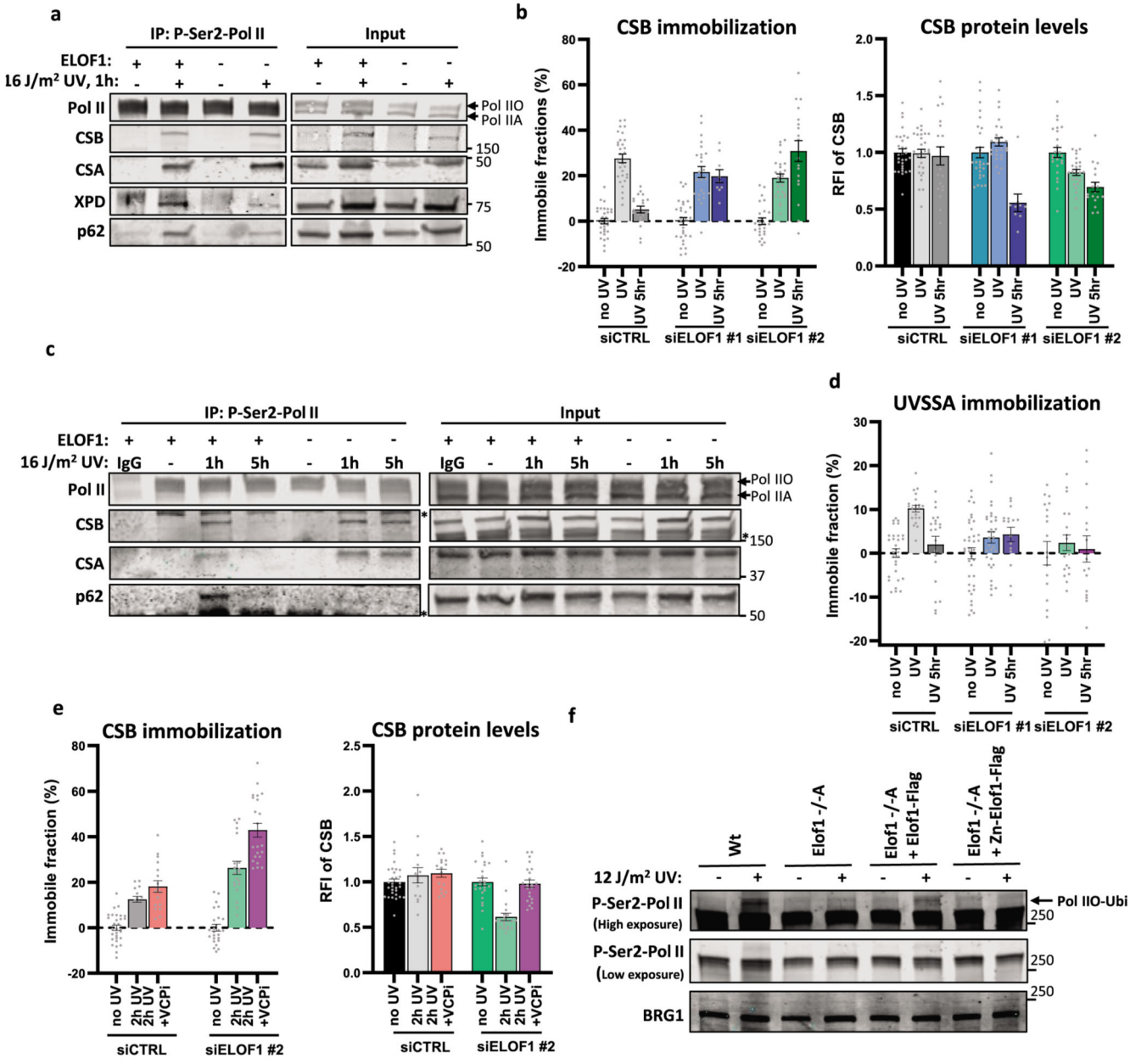

Figure 6. ELOF1 is crucial for proper TC-NER complex assembly.

(a) Immunoprecipitation of P-Ser2-modified Pol II in Wt and ELOF-/-A cells followed by immunoblotting for indicated proteins. Cells were harvested 1 hour after mock treatment or irradiation with 16 J/m^2 UV-C. **(b)** Left panel: Relative immobile fraction of CSB in *CSB-mScarletI* KI cells transfected with indicated siRNAs directly (UV) or 5 hours after UV-C irradiation (5h UV, 4 J/m^2) as determined by FRAP analysis (Extended data fig. 7e). Right panel: Relative fluorescence intensity of CSB-mScarletI in *CSB*-KI cells transfected with indicated siRNAs as determined by live-cell imaging. Values represent mean ± SEM and are normalized to mock-treated. siCTRL NT+UV n=30, 5h UV n=20; siELOF1#1 NT n=30, UV n=25, 5h UV n=9; siELOF1#2 NT+UV n=25, 5h UV n=18 cells analyzed across 2

independent experiments, siELOF1#1 5hr UV was performed once **(c)** Immunoprecipitation of P-Ser2-modified Pol II in Wt and ELOF-/-A cells 1 or 5 hours after UV-C (16 J/m^2) irradiation followed by immunoblotting for indicated proteins. IgG was used as binding control. *non-specific band. **(d)** Same as left panel of (b) but for *UVSSA-mScarletI* KI cells (Extended data fig. 7f,g). siCTRL NT n=30, UV+5h UV n=21; siELOF1#1 NT n=38, UV n=34, 5h UV n=16; siELOF1#2 NT+UV n=19, 5h UV n=16 cells analyzed across 2 independent experiments. **(e)** Relative immobile fraction (left panel) or relative fluorescence intensity (right panel) of CSB-mScarletI in *CSB*-KI cells transfected with indicated siRNAs 2 hours after UV-C irradiation (4 J/m^2) as determined by FRAP analysis (Extended data fig. 7h). VCPi: treatment with VCP inhibitor. Vvalues represent mean ± SEM and are normalized to mock-treated. siCTRL: NT n=30, 2h UV n=15, 2h UV+VCPi n=17; siELOF1#2: NT n=25, 2h UV n=20, 2h UV+VCPi n=22 cells analyzed across 2 independent experiments. **(f)** Immunoblot of chromatin fraction of indicated HCT116 Wt or ELOF1 KO cells, with re-expression of Wt of Zinc-finger mutant ELOF1, 1 hour after 12 J/m^2 UV-C or mock treatment. Loading control; BRG1. Data shown in a, c, f has been performed 2 times with similar results. Numerical data and uncropped blots are provided in source data fig. 6.

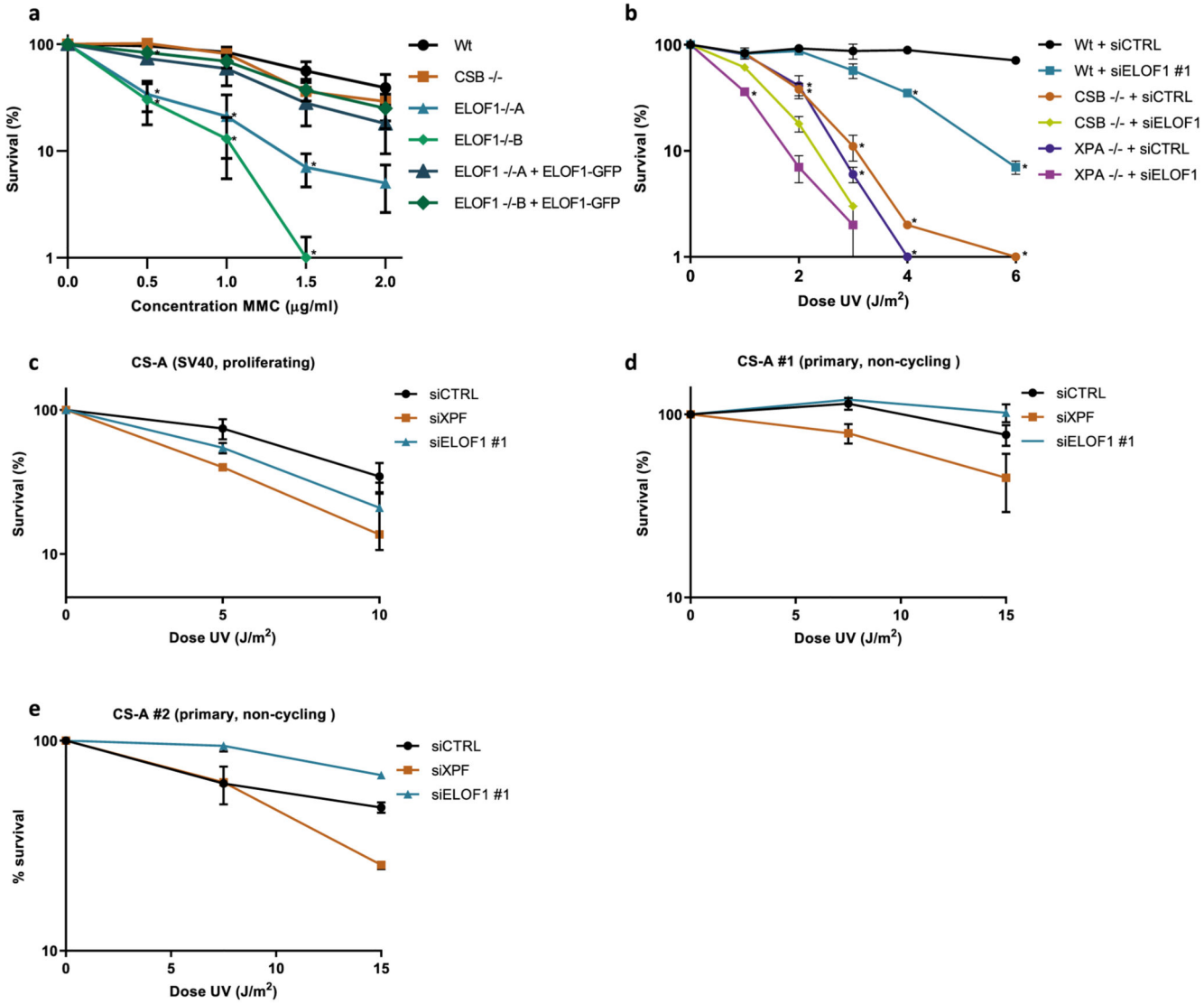

Figure 7. ELOF1 has an additional function apart from TC-NER.

(a) Relative colony survival of indicated HCT116 Wt and KO (-/-) cells, with ELOF1 re-expression where indicated, upon a 1-hour exposure to the indicated concentrations of mitomycin C. Plotted curves represent averages of n=3 independent experiments ± SEM. *P≤0.05 relative to Wt analyzed by one-sided unpaired T-test. **(b)** Relative colony survival of MRC-5 Wt or indicated KO (-/-) cell lines, transfected with indicated siRNAs following exposure to the indicated doses of UV. Plotted curves represent averages ± SEM. *P≤0.05 relative to Wt analyzed by one-sided unpaired T-test. Wt cells n=4 independent experiments, except for 1 and 3 J/m^2 n=3 independent experiments; CSB cells n=3 independent experiments, except for 1 and 3 J/m^2 n=2 independent experiments; XPA cells n=3 independent experiments. **(c)** Viability of replicating CS-A (SV40) or non-replicating primary **(d)** CS216LV (CS-A#1) or **(e)** CS1SP cells (CS-A#2) following exposure to the indicated UV-C doses as determined by AlamarBlue staining. Plotted curves represent averages ± SEM. SV40: siCSA n=2 independent experiments, all other conditions n=3

Europe PMC Funders Author Manuscripts

independent experiments. hTert, CS216LV: n=2 independent experiments for all conditions. hTert, CS1SP: n=2 for all conditions. Numerical data are provided in source data fig. 7.

Europe PMC Funders Author Manuscripts

Europe PMC Funders Author Manuscripts

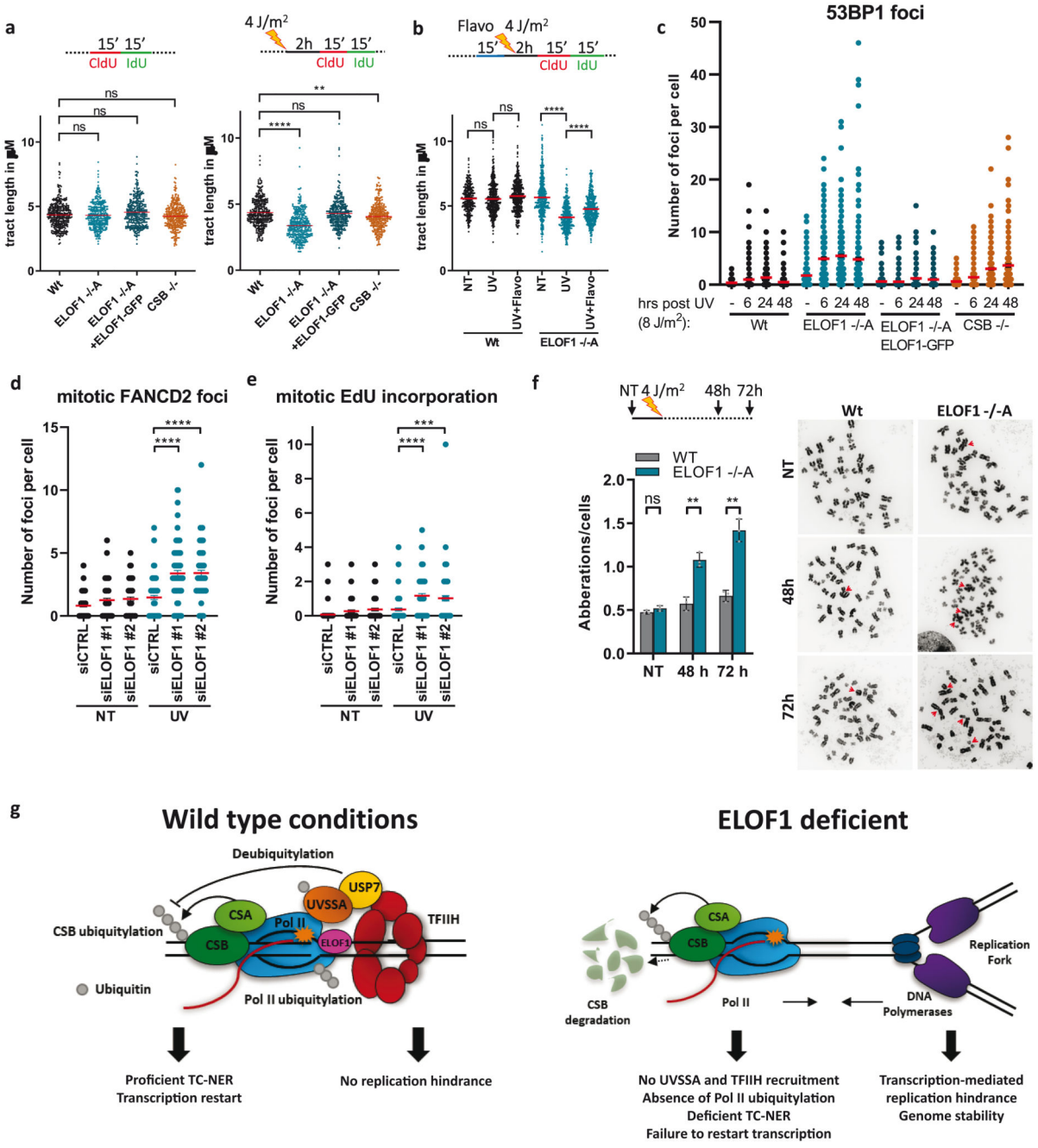

Figure 8. ELOF1 is important for preventing genome instability

(a) Fork progression measured by tract lengths in µm of CldU (red) in indicated HCT116 cells, in untreated conditions (left) or 2 hours after 4 J/m^2 UV-C (right). Tracts of respectively n=347, 343, 348, 341, 347, 335, 336, 339 cells collected from three independent experiments. **(b)** As (a) 2 hours after 4 J/m^2 UV-C with or without 15 min pre-treatment with 0.1 µM flavopiridol (Flavo), of respectively n=355, 510, 506, 506, 508, 535 cells. **(c)** Number of 53BP1 foci in indicated HCT116 cells, untreated or at the indicated timepoints after UV-C (8 J/m^2). Red lines indicate average foci number ± SEM of respectively n=344,

Europe PMC Funders Author Manuscripts

308, 320, 277, 292, 279, 280, 276, 279, 292, 255, 262, 330, 330, 331, 242 cells collected from two independent experiments. **(d)** Number of FANCD2 or **(e)** EdU foci per RPE-1 TP53-/- cell transfected with indicated siRNAs in untreated conditions or 48 hours after irradiation with 4 J/m^2 UV-C. siCTRL NT n=89, siELOF1#1 NT n=91, others n=90 cells analyzed across 3 independent experiments. **(f)** Left: Chromosomal aberrations per cell in HCT116 Wt and ELOF1-/-A cells 48 or 72 hours after 4 J/m^2 UV-C or mock treatment (NT). Data represent average ± SEM of n = three independent experiments. Right: Representative images of metaphase spreads. Arrows indicate chromosomal aberrations. Scale bar: 10μm **(g)** Model showing function of ELOF1. Left: Wild type conditions, ELOF1 is an integral part of the elongation complex and binds near the DNA entry tunnel and ubiquitylation site of Pol II to promote TC-NER and subsequent transcription restart, not resulting in replication problems. Right: in absence of ELOF1, CSA and CSB are still recruited to lesion-stalled Pol II, however, UVSSA, TFIIH, and Pol II ubiquitylation are absent, resulting in TC-NER deficiency and prolonged Pol II stalling resulting in increased transcription-mediated replication hindrance leading to genome instability. *p≤0.05, **≤0.01, *** p≤0.001, ****p≤0.0001, ns non-significant, analyzed by Kruskal-Wallis test for multiple comparisons (a,b), two-sided unpaired t-test (Mann-Whitney) (d,e) and by two-sided unpaired t-test with Welch's correction (f). Numerical data are provided in source data fig. 8.